Performance Modeling and Optimization of Connected and Autonomous Vehicles with Reliable Wireless Connectivity

Haider Shoaib

A thesis submitted to the
Department of Electrical Engineering and Computer Science
in conformity with the requirements for
the degree of Master of Applied Science

YORK UNIVERSITY
TORONTO, ONTARIO

April 2023

Abstract

Vehicle-to-infrastructure (V2I) communication contributes to safe and efficient mobility of connected autonomous vehicles (CAVs). In fully automated traffic streams, speed optimization of CAVs is a fundamental challenge. On one hand, increasing the CAVs' speed improves traffic flow, whereas, on the other hand, it increases communication handovers as the CAVs switch from one base station (BS) to another, thus reducing communication data rates. Therefore, a trade-off exists between the communication data rates and CAV traffic flow.

In the first part of the thesis, we answer the question of determining the optimal active BS density which maximizes the traffic flow subject to CAVs' data rate constraints. Specifically, the proposed framework is designed to (i) maximize the average traffic flow through an aggregate macroscopic traffic flow model while optimizing the active BS density and average CAV speed with network connectivity constraints, and (ii) optimize individual CAV speeds to maximize average traffic flow through a microscopic traffic flow model. We derive closed-form optimal solutions for the active BS density and CAVs' speed using macroscopic model. Our numerical results validate the accuracy of the derived expressions, highlights the enhanced performance of microscopic speed optimization, and extract useful insights related to the impact of CAV's data rate requirements and active BS density on the CAVs' traffic flow. For

instance, increasing the active BS density or lowering the data rate requirements of CAVs enhances the data rates which increases CAV speeds and in turn the traffic flow.

In the second part of the thesis, we extend the system model to include interference and consider the Rayleigh fading channel in the data rate formulation. We derive novel closed-form expressions for outage probability and ergodic capacity of HO-aware data rate, consider that the CAV spacing is log-normally distributed, and we optimize macroscopic traffic flow. Our numerical results validate the accuracy of the outage probability and ergodic capacity expressions, and demonstrate useful insights regarding the impact of HO-aware data rate. For instance, higher CAV speeds results in higher probability of outage, and considering interference results in lower traffic flow compared to traffic flow without the consideration of interference.

The GitHub repository for the contents of this thesis is available at: https://github.com/haidershoaib/Thesis

Acknowledgments

First and foremost, I would like to express my gratitude to my supervisor Professor Hina Tabassum for her immense support and guidance during my undergraduate and graduate studies. Her passion for wireless communications allowed me to develop my own interest and her reviews, insightful comments, encouragement, and guidelines helped me progress and inspire my research work. Furthermore, I would like to thank Professor Mehdi Nourinejad for collaborating with me on my research work. His advice and guidance was very helpful throughout my graduate studies. I would also like to thank my thesis committee members, Dr. Manos Papagelis and Dr. Gunho Sohn for reviewing my thesis and providing helpful feedback.

I would also like to thank my colleagues from the NGWN lab, Mohammed Amin Saeidi, Jeet Tilara, Zijiang Yan, Sadeq bani Melhem, Mehrazin Alizadeh, Borna Barahimi, Dr. Ahmed Al-habob, and Dr. Sylvester Aboagy. Their support and guidance during our group meetings helped me improve the quality of my work and presentations, and provided me with helpful feedback from their own experiences.

Finally, I would like to thank my father, mother, and sister, Shoaib Halim, Rashda Rafiq, and Hira Shoaib for all their encouragement and support and love during my studies. I would also like to thank my uncle Dr. Rashid Bashir for his guidance and support throughout my entire education. I would like to thank my grandparents who

always inspired me to go further in my education. Lastly I would like to thank all of my friends and family who helped me through the thick and thin to get me to where I am today.

Contents

List of Figures

List of Abbreviations

CAV Connected and Autonomous Vehicle

BS Base Station

V2V Vehicle-to-Vehicle

V2I Vehicle-to-Infrastructure

5G Fifth generation

6G Sixth generation

QoS Quality of service

RF Radio Frequency

GHz Gigahertz

THz Terahertz

Bps Bits per second

SNR Signal-to-Noise Ratio

SINR Signal-to-Interference-plus-Noise Ratio

HO Handoff

PDF Probability Density Function

CDF Cumulative Distribution Function

OP Outage Probability

Chapter 1

Introduction

Autonomous driving is an emerging and prominent technology to enhance traffic flow, safety [2], and fuel efficiency [3], while creating new ways of sharing vehicles [2]. By 2030, the global automated driving market's worth is expected to exceed US$173.15 billion. To date, most connected and autonomous vehicles (CAVs) leverage onboard sensors, which build a map of the vehicle's environment, and a control subsystem that governs the longitudinal and lateral motion of vehicles [4]. However, CAVs suffer from the limited range of onboard sensors that only enable detecting adjacent vehicles, thus limiting the ability to efficiently perform complex maneuvers. In this context, vehicle-to-infrastructure (V2I) communication is critical for coordinated driving, access to real-time traffic and navigation information, and informed decision-making through cooperative sensing and maneuvering [4, 5].

The development of 5G and 6G next generation networks is key to the advancement of CAVs. Communication networks that foster lightning-fast data transfer speeds with virtually zero latency, enable CAVs to communicate with one another and with other devices in real-time, making it possible for them to operate safely and efficiently. Next generation networks will also allow for massive amounts of data

to be transmitted and processed at once, enabling vehicles to make split-second decisions based on a wealth of information, from road conditions to weather patterns. With the implementation of next generation networks, we can expect connected automated vehicles to become more reliable and intelligent, leading to improved road safety, reduced traffic congestion, and a more seamless driving experience. Currently, in the Greater Toronto Area, wireless base stations (BSs) are deployed along the major highways (i.e., 401, 403, and 407) sporadically [6]. This method of deployment results in higher latency and poor quality of service (QoS) while travelling along the highways which can severely impact the data rates between BSs and CAVs.

Therefore, V2I communications and their active deployment are important to consider, because if they are not handled properly, they can cause traffic accidents when coordinating messages to groups of far-off vehicles. Although vehicle-to-vehicle (V2V) communications are useful for exchanging information such as headway, speed, and location of CAVs within a small area, V2V communications are generally distance-limited. On the other hand, V2I communications provide a larger range of service to CAVs which can be critical when there are fewer or limited amount of CAVs travelling on the road.

To enable V2I connectivity, the infrastructure consists of BSs that provide the required connectivity for the CAVs as shown in Fig. 1.1. On the one hand, increasing the CAVs' speed results in frequent switching (or handoffs) among BSs which deteriorates communication and lowers the data rate (defined as number of bits transmitted per second) between CAVs and BSs. On the other hand, increasing the CAVs' speed improves the road traffic flow. Thus, a fundamental trade-off exists between the achievable wireless data rates and CAV traffic flow.

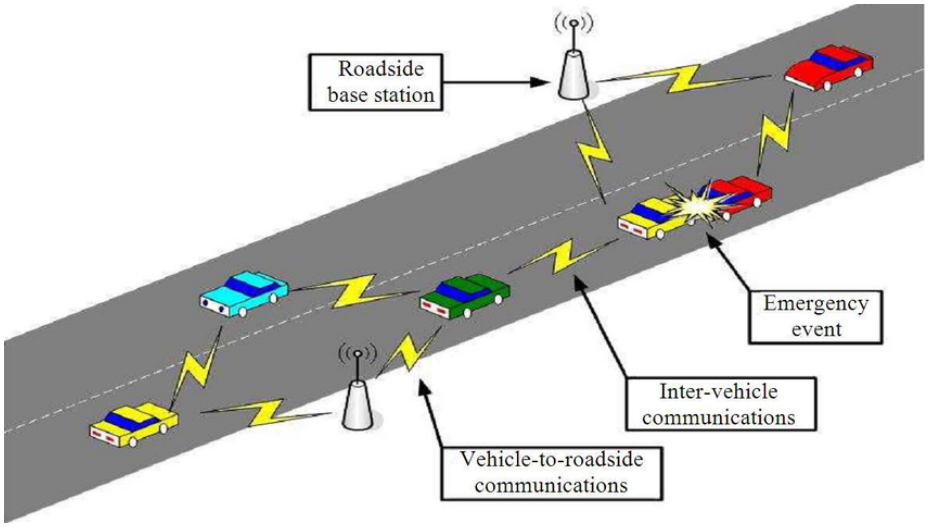

Figure 1.1: Illustration of different types of vehicle communications [1].

Moreover, in conventional non-CAV traffic, empirical evidence shows that the average speed decreases where the vehicle density is larger than the critical density, due to induced friction in mobility [7]. In contrast, the average speed in CAV traffic is also subject to telecommunications restrictions and can be controlled by centralized or decentralized V2I communications with the objective of maximizing traffic flow.

1.1 Mobility Models in Wireless Networks

Mobility-Aware Wireless Networks are typically modeled using mobility models which can simulate the movement of mobile users such as UAVs, CAVs, etc. The two general type of mobility models are trace-based models and random models, where the former refers to the models which utilize real-world data from BSs with actual user locations, and the former refers to spatio-temporal models which are mathematical frameworks that simulate user movements in a random manner.

1.1.1 Trace-based Mobility Models

Trace-based Mobility Models are traditional models which are obtained by measurements of currently deployed systems, which contain connectivity logs and location information of users [8]. Since these models utilize data from deployed systems, they are typically realistic in terms of the movement of the users as well as the topology of the surrounding area. For example, the CRAWDAD Project [9] was established in 2004 as a place to provide datasets across the research community which consists of data captured from wireless networks and the users. Although traces are valuable in terms of assessing performance or handoff protocol optimization, this model is not widely popular in the research community due to the fact that the traces from the data does not generalize well when formulating benchmark results since the data is specific to particular locations.

1.1.2 Random Synthetic Mobility Models

Random Synthetic Mobility Models are mathematical-based models which characterize movement of mobile users. Although these models are simple and analytically tractable, they do not reflect realistic user mobility [10] as compared to *Trace-based Mobility Models*. Some examples of such mathematical models include Bayesian models which have the feature to mimic random behavior of a node or a group of nodes, Brownian motion [11] which characterizes diffusion of small particles with mean transition times and pause times between transitions, and finally the Levy pattern [12] which is known to be more diffusive than Brownian motion, and can approximate human walking patterns in outdoor scenarios. Overall, random mobility models are useful to model mobility in wireless networks due to their analytical tractability and

generalization, which results in the ability to perform mathematical analysis and network optimization, however these models lack realistic movements which are present in *Trace-based Mobility Models*.

Random Synthetic Mobility Models can be characterized into individual and group mobility models.

- In *Random Individual Mobility Models*, one type of models are memoryless, which has no spatio-temporal correlation [13]. In these types of models, users move without the knowledge of other users, and the location and speed of a user is not influenced from other users. These models are known to be tractable, however in the context of CAVs, there is a higher chance of collisions, if a CAV does not have any knowledge about any surrounding CAVs. Furthermore, there are models with memory which have temporal correlation [13]. In these models, a user is still not aware of other users, however the location and speed of a user is influenced by its previous locations and speeds.

- *Random Group Mobility Models* use mathematical functions to describe the mobility of a group of users, such as the exponential correlated random mobility model [13], community model, and column mobility model [14]. These models simulate the behaviour of a group of users moving together, such as in a line and move in a certain direction in the column mobility model, or users following the behaviour of a leader node in reference point group mobility models [15]. Overall, group mobility models are more useful when considering CAVs and traffic flow, since the users are aware of the other users and there are less chances of collisions compared to *Random Individual Mobility Models*.

1.2 Vehicle Traffic Flow Models

Vehicle Traffic Flow Models are somewhat synonymous to group mobility models. That is, the traffic flow models are typically represented using car-following models [16] where a following vehicle is aware of the distance between itself and its leader vehicle. On the other hand, in group mobility models [14], several nodes group together in a platoon with a leader node, and the nodes change their positions according to a random distribution such as exponential, and are not aware of other platoons, which may cause collisions. Furthermore, the formulation of random group models lacks the safety distance metric. Therefore, car-following models are more practical models when analyzing traffic flow in mobility models.

There are three types of traffic flow models considered in transportation research, which include macroscopic, microscopic, and mesoscopic traffic flow models.

1.2.1 Macroscopic Traffic Flow

Traffic flow models have been developed since the early 2000s which helped in modelling and predicting traffic flow. For instance, Papageorgiou [17] contributed to the discussion of macroscopic traffic flow modelling, where macroscopic models assume a sufficiently large number of vehicles on a road such that each stream of vehicles can be treated as flowing in a tube or a stream [18]. Papageorgiou emphasized the fact that macroscopic models are useful for traffic engineering tasks such as simulation and planning, however they lacked in validation results and practical applications which required highly accurate results to predict and model traffic flow.

1.2.2 Microscopic Traffic Flow

On the other hand, microscopic traffic flow models describe the details of traffic flow and the interaction taking place within it considering single vehicle-driver units. The dynamic variables of the model represent microscopic properties like the position and speed of individual vehicles [18]. The most famous microscopic car following models are classified as safe-distance models which includes Pipe's model, Forbes' model, and General Motor's model [16]. Each model demonstrates how one vehicle follows another, and the models vary in how the driver reacts by using metrics such as reaction time and safety distance or safety speed.

1.2.3 Mesoscopic Traffic Flow

Furthermore, a combination of macroscopic and microscopic models are known as mesoscopic traffic flow models. For instance, in [19], Bagnerini et al. introduced a mesoscopic model which accounted for the behaviour of different types of vehicles where the traffic was defined as a continuum flow, but also analyzed each individual vehicle behavior. Finally, the concept of the fundamental diagram of traffic flow [20] is widely used when describing the relation between traffic flow and traffic density. As the traffic density increases, the traffic flow increases up to a certain point, and begins to decrease when the traffic density attains large values, which means the vehicles lower their speeds due to traffic congestion.

1.3 Research Gaps

Overall, the traffic flow models are useful when analyzing traffic flow, where macroscopic models provide statistically averaged results, while assuming traffic flow as a

stream, whereas microscopic models enables incorporating the details of individual CAVs and optimize an individual CAV speed. The traffic flow models however do not incorporate the dynamics of speed and CAVs' connectivity to BSs, where the network connectivity can potentially influence CAV speeds in order to meet a required minimum data rate when considering V2I communications in the traffic flow models.

On the other hand, the mobility models applied in wireless networks literature are useful when assessing handoff rates and sojourn time. The *Trace-based Mobility Models* are useful when analyzing real-world data and obtaining realistic results, however the results do not generalize well and the data is typically difficult to obtain. On the other hand, *Random Synthetic Mobility Models* are useful in research since they generalize well, however the user movements are not realistic, so the results may not be accurate in the real-world. The gap in current mobility models is that they do not typically consider traffic flow and car-following models for CAVs, and how to optimize speed and traffic flow in vehicular networks

1.4 Challenges

Some of the primary challenges in modeling and optimizing mobility-aware wireless networks while considering vehicle traffic flow are listed below:

- **Active BS density:** In a traffic flow model where CAVs connect to the nearest BS, the active BS density on the road is a crucial factor. For instance, fewer deployed BSs may not be able to provide an adequate quality of service to the CAVs, thus the CAVs will travel at lower speeds which results in reduced traffic flow. On the other hand, if there are too many BSs deployed on the road, this leads to an increase rate of handoffs (switching between BSs), which lowers the

data rate between the CAV and BS, thus lowering the CAV speed. Therefore, in order to solve this issue, an optimal number of BSs needs to be deployed with respect to the network parameters of the system.

- **Handoff-aware Data Rate:** In vehicular communications, it is important to characterize the data rate between a CAV and BS in terms of the handoff rate since the data rate is a function of the number of BSs switching. Arshad et al. [21] derived an expression for handoff-aware data rate which provides the connection between speed and data rate through the handoff rate, where handoff rate is defined as the number of cell boundaries crossed per second. Although the handoff-aware data rate solves the issue for constantly moving CAVs, this metric alone does not account for traffic flow and does not incorporate the dynamics of the surrounding CAVs.

- **Safety Distance in Traffic Flow Models:** In vehicle traffic flow models, the car-following model is typically used. In these models, CAVs aim to maintain a safety distance [22], i.e., a predefined distance between a follower and leader which ensures collision avoidance. The gap in current traffic flow models is that they do not consider network connectivity to BSs, and handoff-aware data rates are not accounted for when determining the speed that a CAV should maintain to not only travel at safe speeds, but to also maintain an adequate quality of service when connected to BSs.

1.5 Scope of the Thesis

This thesis provides a comprehensive framework to jointly optimize the active BS density and CAV speeds while taking network and transportation constraints into

account. The contributions are as follows:

- We develop a novel optimization framework to jointly optimize the active BS density and speed of CAVs in order to maximize the CAVs' traffic flow with collision avoidance and minimum handoff-aware data rate constraints. The traffic flow has been modeled using both the macroscopic and microscopic models. The macroscopic model enables analytical tractability and is suitable for long-term decision making problems like network deployment; whereas the microscopic model enables optimizing the instantaneous CAV's speed individually and their interactions with other CAVs.

- Considering the macroscopic model, we formulate traffic flow maximization while optimizing average speed of CAVs and active BS density along the CAVs' corridor. We derive closed-form expressions for traffic flow as well as closed-form optimal solutions for the CAV's speed and the number of BSs deployed along the corridor considering a high signal-to-noise ratio (SNR) regime.

- In the microscopic model, we formulate traffic flow maximization to optimize each CAV's speed individually and use the optimal density of BSs calculated from the macroscopic model as the deployment of BSs is a long-term decision problem.

- Our simulation results confirm the accuracy of the derived closed-form expressions. Our results analyze the sensitivity of the important communication and CAVs network parameters such as CAVs' minimum data rate requirements, density of BSs, wireless channel propagation, etc. and extract useful insights related to the optimal CAVs' speed and active BS density.

- We extend the framework to characterize macroscopic traffic flow by considering log-normal distribution of the spacing between CAVs. Then, we derive novel and tractable closed-form expressions for the probability density function (PDF) and cumulative density function (CDF) of signal-to-interference-plus-noise ratio (SINR), HO-aware rate outage probability (OP) and ergodic capacity in a large-scale network with interference. The derived expressions capture the network parameters such as height of the BSs, safety distance of BSs from the road, interference from neighboring BSs, and channel fading.

1.6 Research Outcome

- H. Shoaib and H. Tabassum, "Optimization of Speed and Network Deployment for Reliable V2I Communication in the Presence of Handoffs and Interference," *IEEE Wireless Communication Letters*, 2023 (accepted).

- H. Shoaib, M. Nourinejad, and H. Tabassum, "Macroscopic Traffic Flow Analysis and Optimization with V2I Connectivity and Collision Avoidance Constraints," *IEEE International Conference on Communications*, 2023 (accepted).

- H. Shoaib, M. Nourinejad and H. Tabassum, "Performance Optimization of Connected Automated Vehicles With Handoff-Aware Communications," submitted.

Chapter 2

Mathematical Preliminaries and Literature Review

2.1 Key Performance Metrics

The Traffic Flow, SNR, SINR, data rate, OP, and ergodic capacity are all essential performance metrics to assess the performance of the traffic flow model with network constraints. This section consists of a preliminary review of the aforementioned metrics to understand the performance of traffic flow models with wireless networks.

2.1.1 Traffic Flow

According to traffic flow theory, the fundamental diagram is defined as the traffic flow as a function of the density of vehicles on the road and includes the average vehicle speed [23]. Traffic flow can be defined as follows:

$$q = kv, \tag{2.1}$$

where q is the traffic flow measured in vehicles per unit time, k is the vehicle density measured in vehicles per unit distance and v is the average vehicle speed.

2.1.2 Signal to Noise Ratio (SNR) and with interference (SINR)

The received signal power from a typical RF (radio frequency) BS to a user [24] is defined as follows:

$$S_{i,j} = G_R^{\text{tx}} G_R^{\text{rx}} \left(\frac{c}{4\pi f_R} \right)^2 \frac{P_j^{\text{tx}}}{d_{i,j}^{\alpha}} \chi_{i,j} = \gamma_R P_j^{\text{tx}} d_{i,j}^{-\alpha} \chi_{i,j}, \tag{2.2}$$

where G_R^{tx} and G_R^{rx} represent the transmitting and receiving antenna gains, respectively, P_j^{tx} represents the transmit power of the BS j, $\chi_{i,j}$ represents the short-term channel fading of BS j, c and f_R represent the speed of an electromagnetic wave and RF carrier frequency, respectively, $d_{i,j}$ represents the distance between the j-th BS and i-th user, and α represents the path-loss exponent. Therefore, the SNR can be calculated as follows

$$\text{SNR}_{i,j} = \frac{S_{i,j}}{N_R}, \tag{2.3}$$

where N_R is the thermal noise at the receiver. Finally the SINR can be defined as follows:

$$\text{SINR}_{i,j} = \frac{S_{i,j}}{I_i + N_R}, \tag{2.4}$$

where $I_i = \sum_{k \neq j} P_k^{\text{tx}} \gamma_R d_{i,k}^{-\alpha} \chi_{i,k}$ is the cumulative interference at user i from the interfering BSs measured in watts.

2.1.3 Data Rate

According to the mathematical theory of communications, Claude Shannon developed the channel capacity called the Shannon-Hartley theorem [25] which is used widely in information theory. The Shannon-Hartley theorem provides the maximum rate and which information is transmitted over a an additive white Gaussian noise (AWGN)

channel. The data rate is defined as follows:

$$C = W_c \log_2 (1 + \text{SINR}), \tag{2.5}$$

where C is the channel capacity in bits per second (bps), W_c is the bandwidth of the channel in Hz. It is worth noting that both SNR and SINR can be used to calculate the channel capacity.

2.1.4 Handoff Rate

A handoff occurs when a user switches from one BS to another. There are two types of handoffs including horizontal and vertical handoffs. A horizontal handoff occurs when the user switches from one BS to another similar BS (eg. RF to RF), and a vertical handoff occurs when the user switches from one BS to a different type of BS (eg. RF to THz). Handoff rate is defined as the average number of handoffs divided by the average time it takes for a user to move from one location to the other [26]. Handoff rate can be mathematically defined as follows:

$$H = \mathbb{E}[\text{Number of handoffs per unit time}]. \tag{2.6}$$

2.1.5 Outage Probability

Outage Probability (OP) is the probability that a given information rate is not supported by the channel. The OP of SINR of a channel is less than or equal to a certain threshold [24] can be defined as follows:

$$P_{\text{out}} = P(\text{SINR} \leq \gamma_{\text{th}}), \tag{2.7}$$

where γ_{th} is the SINR threshold.

2.1.6 Ergodic Capacity

Ergodic capacity is a performance metric which is defined as the highest data rate at which information can be sent over a channel with little probability of error [27]. Ergodic capacity can be defined as follows:

$$C_{\text{avg}} = \mathbb{E}\left[\log_2\left(1+Z\right)\right] = \int_0^\infty \log_2(1+Z) f_Z(z) dz, \tag{2.8}$$

where Z is the SINR, and $f_Z(z)$ is the pdf of the SINR.

2.2 Mathematical Preliminaries

In this section, a series of mathematical preliminaries are discussed so that readers can comprehend the discussions in the following chapters. We present topics including random variables, Probability Density Function (PDF), Cumulative Distribution Function (CDF), and single random variable transformation.

2.2.1 Probability Density Function (PDF)

The Probability Density Function (PDF) is a statistical measure which demonstrates the probability distribution of a random variable X. It can provide the probability that the value of a random variable will land between a given interval as follows:

$$\Pr[a \leq X \leq b] = \int_a^b f_X(x) dx, \tag{2.9}$$

where X is a random variable. Some common PDFs include normal distribution, exponential distribution, Poisson distribution, etc.

2.2.2 Cumulative Distribution Function (CDF)

The Cumulative Distribution Function (CDF) is a statistical measure which evaluates the probability of a random variable X less than or equal to a certain value x as follows:

$$F_X(x) = \Pr(\mathrm{X} \leq \mathrm{x}). \tag{2.10}$$

Furthermore, the CDF function $F_X(x)$ can be derived using the PDF of X as follows:

$$F_X(x) = \int_{-\infty}^{x} f_X(t)dt. \tag{2.11}$$

2.2.3 Single Random Variable Transformation

For given random variable X, and another random variable Y such that $Y = g(X)$, where g is a one-to-one function, the PDF of the transformed random variable Y can be calculated as follows:

$$f_Y(y) = f_X(g^{-1}(y)) \left| \frac{d}{dy} g^{-1}(y) \right|, \tag{2.12}$$

where $f_X(\cdot)$ is the PDF of X. More details regarding probability and statistics theory can be found in [28].

2.2.4 Optimization

A constrained optimization problem is a problem which finds the optimal feasible solution given certain constraints as follows:

$$\begin{aligned} \min_{x} \quad & f(x) \\ \text{s.t.} \quad & g_i(x) \leq 0, \quad i = 1, \ldots, m \\ & h_j(x) = 0, \quad j = 1, \ldots, p \end{aligned} \tag{2.13}$$

where $f(x)$ is the objective function which is minimized over x, $g_i(x) \leq 0$ is known as an inequality constraint, and $h_j(x) = 0$ is known as an equality constraint. There are different methods to solve constrained optimization problems such as linear programming, nonlinear programming, and the Karush–Kuhn–Tucker approach. The details of these approaches can be found in [29].

2.3 Literature Review

2.3.1 Wireless Communications with Mobility

From telecommunication research perspective, road-traffic flow considerations with macroscopic or microscopic car following models have been predominantly overlooked. That is, the existing research works only consider the data rate as a function of speed without quantifying its impact on traffic flow. In [21] and [30], Arshad et al. presented speed-aware handoff management schemes and derived the expressions for handoff-aware data rates using stochastic geometry. In [31], Ibrahim et al. shed light on the handoff problem in the context of C-plane and U-plane split architecture. The CP/UP architecture enables users to receive data packets from a nearby small base-station

(SBS) while also being controlled by a macro base-station (MBS) which is further away, which reduces control overhead when compared to traditional architectures. The authors of this paper derived expressions for per-user mobility-aware data rate (which is a function of handoffs) using stochastic geometry tools. In [32], Lin et al. proposed a random way-point mobility model to characterize the handoff rate and sojourn time using stochastic geometry considering randomly distributed BSs. Recently, in [24], Hossan et al. developed a stochastic geometry framework to analyze the performance of a mobile user in a two-tier wireless network operating on sub-6GHz and Terahertz (THz) frequencies. The authors characterized the overall handoff probability, coverage probability, and most importantly derived the mobility-aware probability of coverage of a mobile user in a hybrid RF-THz network setup. Recently, in [33], Yan et al. proposed a reinforcement learning approach for joint V2I network selection and autonomous driving policies considering both RF and THz BSs. Their results demonstrated inter-dependency of a CAV's motion dynamics, HOs, and data rate to adopt safe driving behaviours for CAVs.

2.3.2 Traffic Flow Analysis

Transportation network performance is commonly characterized in terms of traffic flow efficiency assuming either macroscopic, microscopic, or mesoscopic car-following models, where the latter refers to a hybrid of the macroscopic and macroscopic models. Furthermore, *V2I network connectivity* with respect to wireless network operations are seldom considered in traffic flow models. For instance, Shi et al. [23] proposed

a general methodology for CAVs consisting of the combination of empirical and theoretical experiments to construct fundamental diagrams, which demonstrate the relationship between traffic flow and vehicle density. In [34], Jiao et al. extended the car-following model to incorporate V2V communications. They presented an optimal speed equation considering safe space headway and the speed of the preceding vehicle, and the results demonstrated improved CAV mobility in a variety of traffic scenarios. Recently, Nourinejad et al. [35] investigated the trade-offs in the values and costs of individual versus cooperative sensing for CAVs. They formulated two non-linear programming problems to determine the optimal investment in corridor capacity in the long-term, and maximize social welfare in the short-term through road pricing. The flow-density results were presented for different connectivity levels and sensor ranges.

References	**Objective**	**Approach**	**Comments**
[36, 37]	Handoff optimization	Analytical	Simulation based
[38–40]	Handoff optimization	Algorithms	Simulation based
[24, 41, 42]	Coverage probability, Handoff analysis	Analytical	Trajectory based
[43, 44]	Traffic flow analysis	Analytical	Simulation based
[45]	Traffic flow optimization, Road network analysis	Algorithms	Simulation based

[46, 47]	Traffic flow optimization, V2V analysis	Algorithms	Simulation based
[48]	Traffic flow optimization, Road network analysis	Algorithms	Markov-chain based

Table 2.1: Current Literature in Mobility and Transportation Networks

As shown in Table 2.1, none of the aforementioned research works considered *CAVs traffic flow maximization* with *handoff-aware network connectivity* constraints and *collision avoidance* constraints. Specifically, most of the transportation research have overlooked the interdependency of the CAVs' mobility, including speed, handoffs, and wireless data rates, whereas most of the telecommunication research did not consider the traffic flow dynamics.

Chapter 3

Traffic Flow Maximization with Handoff-Aware Data Rate Constraints

V2I communications are important to consider for CAVs to ensure the required network connectivity. However, increasing the CAVs' speed results in frequent handoffs among BSs which deteriorates the data rate between CAVs and BSs. On the other hand, increasing the CAVs' speed improves the road traffic flow. Thus, a fundamental trade-off exists between the achievable wireless data rates and CAV traffic flow. In this context, this paper addresses a critical question of *how to analyze and maximize the macroscopic and microscopic traffic flow by optimizing the speed of CAVs and network deployment such that the CAVs' data rate requirements can be satisfied?*. The contributions of this chapter are as follows:

- We first characterize a closed-form expression of the macroscopic traffic flow by considering exponential distribution of the spacing between CAVs.
- The derived expression for the traffic flow is used to jointly optimize the deployment of BSs and speed of CAVs while maximizing the CAVs' traffic flow with collision avoidance and handoff-aware data rate constraints.

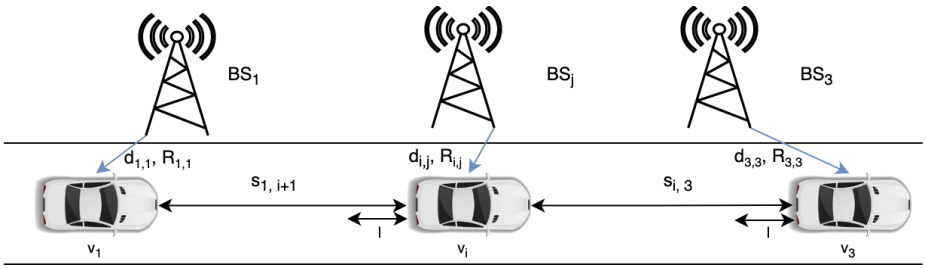

Figure 3.1: Graphical illustration of the CAV to wireless infrastructure communication.

- We derive closed-form optimal solutions for the CAV's speed and the number of BSs deployed along the corridor considering a high signal-to-noise ratio (SNR) regime.

- In the microscopic model, We formulate traffic flow maximization to optimize each CAV's speed individually and use the optimal density of BSs calculated from the macroscopic model as the deployment of BSs is a long-term decision problem.

- Our simulation results confirm the accuracy of the derived closed-form expressions. We analyze the sensitivity of the important communication and CAVs network parameters such as CAVs' minimum data rate requirements, density of BSs, wireless channel propagation, density of vehicles, etc. and extract useful insights related to the optimal CAVs' speed and network deployment.

3.1 System Model and Assumptions

3.1.1 CAV - Traffic Flow Model

We consider a CAV-exclusive corridor equipped with telecommunication BSs that allow transfer of data between each CAV and the network infrastructure. The BSs

are deployed uniformly along the corridor as shown in Fig. 3.1, and have a density μ defined as the number of BSs deployed per unit distance. The CAV density k on the corridor is defined as the number of CAVs per unit distance, and the CAV speed is v. According to macroscopic traffic flow theory, the flow of vehicles is defined as $q = kv$ vehicles per unit time. We assume a given Probability Density Function (PDF) of the density of vehicles k on the corridor and denote it as $f_K(k)$. Subsequently, the traffic flow can be defined as follows:

$$Q = \int_0^\infty kv f_K(k) \mathrm{d}k. \tag{3.1}$$

3.1.2 Network - Data Rate Model without Mobility

Each CAV is assumed to be connected to a single nearest BS at any given time. Considering the distance-based path-loss and short-term multi-path fading at the transmission channel, the received signal power at a given CAV i from a given BS j in the downlink can be modeled as follows:

$$P_{i,j}^{\mathrm{rx}} = G_R^{\mathrm{tx}} G_R^{\mathrm{rx}} \left(\frac{c}{4\pi f_R} \right)^2 \frac{P_j^{\mathrm{tx}}}{d_{i,j}^{\alpha}} \chi_{i,j} = \gamma_R P_j^{\mathrm{tx}} d_{i,j}^{-\alpha} \chi_{i,j}, \tag{3.2}$$

where G_R^{tx} and G_R^{rx} represent the transmitting and receiving antenna gains, respectively, P_j^{tx} represents the transmit power of the BS j, $\chi_{i,j}$ represents the short-term channel fading between the BS j and CAV i modeled with Rayleigh distribution, c and f_R represent the speed of an electromagnetic wave and RF carrier frequency, respectively, $d_{i,j}$ represents the distance between the BS and CAV, and α represents the path-loss exponent. Subsequently, given the Shannon-Hartley theorem for infinite block-length regime [25], the data rate without mobility between a BS and CAV can

be defined as:

$$R_{i,j} = W_c \log_2(1 + \text{SNR}_{i,j}) = W_c \log_2 \left(1 + \frac{\gamma_R P_j^{\text{tx}} d_{i,j}^{-\alpha} \chi_{i,j}}{N_R}\right), \tag{3.3}$$

where SNR denotes signal-to-noise ratio at the reciever, W_c represents the bandwidth of the channel, and N_R is the thermal noise power at the receiver. For simplicity, we assume there is no interference incurred at the CAVs' receivers from the BSs. Furthermore, the data rate between the CAV and BS decreases with distance due to free-space path-loss attenuation, and small-scale fading.

3.1.3 Network - Handoff-Aware Data Rate Model

As CAVs drive along the corridor, they switch from (connecting to) one BS to another, which is called a "handoff." Frequent handoffs can severely impact the received CAV data rate due to handoff latency and handoff failures. Therefore, it is necessary to incorporate the effect of these handoff issues through the handoff-related cost. handoff cost is proportional to the handoff delay (h_d) measured in seconds per handoff, and handoff rate (H) measured in number of handoffs per second [31], i.e.,

$$H_c = h_d \times H, \tag{3.4}$$

Since we assume CAV connection to its nearest BS, H can be defined as the *number of cell boundaries a CAV crosses per second*, where a cell boundary is the coverage range of a BS. Note that the number of boundaries per unit distance are the same as the number of BSs deployed per unit distance defined by μ. Now given the distance covered by CAV in a second (i.e., speed v), we can calculate the number of boundaries

covered by a CAV per second as $H = \mu v$.

Subsequently, we model the handoff-aware data rate [21] as:

$$R_{i,j}^{m} = R_{i,j}(1 - h_d H_{c,\max}) = R_{i,j}\left(1 - h_d \frac{\mu v_i}{\mu_{\max} V_{\max}}\right), \tag{3.5}$$

where $H_{c,\max} = \frac{H}{\mu_{\max} V_{\max}} = \frac{\mu v}{\mu_{\max} V_{\max}}$ is the normalized handoff cost in equation (3.5) to ensure $0 \leq H_{c,\max} < 1$, $\mu_{\max}$ is the maximum regulated active BS density, and $V_{\max}$ is the maximum regulated speed of the CAVs. Finally, a stable CAV connection with the nearest BS requires a minimum handoff-aware data rate R_{th} which ensures that every CAV achieves the required quality of service.

3.2 Macroscopic Traffic Flow Maximization

In this section, we present the average traffic flow maximization problem while ensuring the safety distance/collision avoidance and desired network connectivity of CAVs. We then derive a closed-form representation of the problem considering the statistics of the distance between two CAVs s, where k is inversely proportional to s (i.e. $k = 1/s$). Since the handoff-aware data rate is a function of the CAVs speed, which also affects the CAV traffic flow, we consider optimizing the speed of CAVs. In addition, since the density of BSs directly impacts the handoff-aware data rate in (3.5), we consider optimizing the density of BSs as well. Finally, we present the closed-form solutions of the CAVs speed and active BS density.

3.2.1 Problem Formulation

In the proposed optimization problem (**P1**), we introduce three constraints, stipulating that although an increase in speed will maximize the traffic flow, this speed

must also be lowered to **(i)** achieve a better quality of service on the telecommunications side (through minimizing handoffs), and **(ii)** the CAVs safety distance on the transportation side to avoid possible collisions which would affect the traffic flow. Regarding equation (3.1), we utilize s instead of k considering that s is exponentially distributed [49] with the PDF is $f_S(s) = \lambda \exp(-\lambda(s-l))$ and the cumulative density function (CDF) is given by $F_S(s) = 1 - \exp(-\lambda(s-l))$, where l is the safety distance between two CAVs when they are idle, λ is the average CAV density and $1/\lambda$ is the average spacing between the CAVs. The problem can thus be formulated as:

$$
\begin{aligned}
(\mathbf{P1}) \quad & \max_{v,\mu} \qquad Q = \int_l^{\infty} \frac{1}{s} v \lambda e^{-\lambda(s-l)} \mathrm{d}s \\
\text{s.t.}(\mathbf{C1}) \quad & \Pr\left(v \geq \frac{s-l}{\tau}\right) \leq \epsilon \\
(\mathbf{C2}) \quad & W_c \log_2\left(1 + \bar{\gamma}(2\mu)^{\alpha}\right)\left(1 - \bar{h}_d \mu v\right) \geq R_{\text{th}} \\
(\mathbf{C3}) \quad & 0 \leq v \leq V_{\max} \\
(\mathbf{C4}) \quad & 0 \leq \mu \leq \mu_{\max}
\end{aligned}
$$

where $\bar{h}_d = \frac{h_d}{\mu_{\max} V_{\max}}$ and $\bar{\gamma} = \frac{\gamma_R P_j^{\text{tx}} \mathbb{E}[\chi_{i,j}]}{N_R} = \frac{\gamma_R P_j^{\text{tx}} \chi_0}{N_R}$. Since the transmission channel fading varies in the order of milliseconds compared to the distance between the CAVs and BSs, we consider the average value of the instantaneous channel fading in **(C2)**, i.e., $\chi_0 = \mathbb{E}[\chi_{i,j}]$.

The first constraint (**C1**) is based off the car-following model which states that the speed of the CAVs should not exceed $(s-l)/\tau$, where s is the distance between two CAVs, l is the safety distance between two idle CAVs, τ denotes the processing time required for CAVs to act on a decision, and ϵ is the crash intensity level. The second constraint (**C2**) states that the hand-off aware data rate (3.5) should be greater than

a certain threshold R_{th} which would achieve the minimum required data rate for the CAVs considering the maximum distance between the CAVs and BSs, i.e., $d_{\max} = 1/2\mu$, where the spacing between BSs is $1/\mu$ and the factor of half is because the halfway point between the two BSs defines the network switching boundary. Clearly, considering the maximum distance gives a lower bound on the achievable data rate which is what we incorporated in **(C2)**.

3.2.2 Closed-Form Representation of the Problem

This section discusses the properties of the problem **(P1)** and presents a reformulation of the problem that can be solved through an exact approach. A closed-form expression of the objective function presented in **(P1)** can be obtained using the following identity in [50][3.352/4]:

$$\int_0^\infty \frac{\exp\left(-ax\right)}{x+\beta} dx = -e^{\beta a} E_i(-\beta a) = e^{\beta a}\Gamma(0, \beta a). \tag{3.6}$$

where $E_i(\cdot)$ is the exponential integral function and $\Gamma(\cdot)$ is the upper incomplete gamma function. Furthermore, **(C1)** can be rewritten by substituting the CDF of s where $\Pr\left(v \geq \frac{s-l}{\tau}\right) = 1 - e^{-\lambda\tau v}$. Taking the natural log of both sides and factoring for v, **(C1)** can be rewritten as follows:

$$v \leq \frac{-\log(1-\epsilon)}{\lambda\tau} = V_{\text{safe}}, \tag{3.7}$$

where equation (3.7) indicates that speed is capped to create an adequate safety distance that is traversed during the processing time. We refer to the right side of (3.7) as the maximum safe speed that keeps the crash probability below ϵ. The condition

(3.7) shows that the maximum safe speed increases with the safety confidence level ϵ, but decreases with the processing time and CAV density. Finally, by expanding **(C2)** and factoring out for v we can rewrite **(C2)** as:

$$v \leq \frac{1}{\bar{h}_d \mu} \left(1 - \frac{R_{\text{th}}}{W_c \log_2 \left(1 + \bar{\gamma}(2\mu)^{\alpha}\right)}\right) = V_{\text{data}}(\mu), \tag{3.8}$$

Similarly, we refer to the right side of (3.8) as the maximum compatible speed, denoted by $V_{\text{data}}(\mu)$ that allows a safe data rate between the CAVs and their nearest BSs. To ensure that (3.8) does not attain negative values of speed and the problem remains feasible, we introduce the following constraint:

$$R_{\text{th}} \leq R_s, \tag{3.9}$$

where $R_s = W_c \log_2 \left(1 + \bar{\gamma}(2\mu)^{\alpha}\right)$ and (3.9) ensures that the data rate R_s is always greater than or equal to the data rate threshold, i.e., $\frac{R_{\text{th}}}{W_c \log_2 (1+\bar{\gamma}(2\mu)^{\alpha})} \leq 1$. By factoring out in terms of μ, (3.9) can be rewritten as follows:

$$\mu \geq \frac{1}{2\bar{\gamma}^{1/\alpha}} \left(2^{R_{\text{th}}/W_c} - 1\right)^{1/\alpha} = \mu_{\text{data}} \tag{3.10}$$

This constraint is referred to as **(C4)** in the subsequent optimization problem formulations along with capping the active BS density to $\mu_{\max}$. The original problem is

re-written **(P1)** in closed-form as follows:

$$\begin{aligned}
(\mathbf{P2}) \quad & \max_{v,\mu} \qquad Q = v\lambda e^{\lambda l}\Gamma(0,\lambda l) \\
\text{s.t.}(\mathbf{C1}) \quad & v \leq \frac{-\log(1-\epsilon)}{\lambda\tau}, \\
(\mathbf{C2}) \quad & v \leq \frac{1}{\bar{h}_d\mu}\left(1 - \frac{R_{\text{th}}}{W_c \log_2\left(1+\bar{\gamma}(2\mu)^{\alpha}\right)}\right) \\
(\mathbf{C3}) \quad & 0 \leq v \leq V_{\max} \\
(\mathbf{C4}) \quad & \mu_{\text{data}} \leq \mu \leq \mu_{\max}
\end{aligned} \tag{3.11}$$

Note that Problem **(P2)** is a non-linear programming problem due to constraint **(C2)** which is a non-linear function of both v and μ. The remaining constraints and the objective function are linear w.r.t. speed v or active BS density μ.

3.2.3 Problem Analysis and Proposed Solution

To solve this problem, we present a solution approach inspired by backward induction that singles out a specific decision variable, in this case v. For a given μ, the optimal speed solution can then be given as in the following Lemma.

Lemma 1. *Given that $Q(\mu)$ is linearly increasing with v, and that v is bounded from above by $V_{\max}$, V_{safe}, and V_{data}, the optimal speed $v^*(\mu)$ is derived as the largest feasible speed that does not violate the three constraints, such that*

$$v^*(\mu) = \min\{V_{\max}, V_{\text{safe}}, V_{\text{data}}(\mu)\}. \tag{3.12}$$

Proof. Let $Q(\mu)$ be the maximum flow that is achieved at an optimal average speed

of $v^*(\mu)$. Therefore, the maximum flow is written as follows:

$$Q^* = \max_{\mu} Q(\mu), \tag{3.13}$$

which is achieved at active BS density μ^* and average speed $v^*(\mu^*)$. From the three speed limits, the maximum safe speed V_{safe} depends on the CAV spacing distribution (with parameters λ and l) and the maximum speed for adequate data rate $V_{\text{data}}(\mu)$ depends on the active BS density, which is to be optimized. The maximum speed, $V_{\text{data}}(\mu)$, has the active BS density μ and can have a single maximum (as illustrated in Fig. 1). The implication of this property is that an initial increase in μ increases V_{data} as it allows CAVs to be closer to the BS and acquire a higher data rate. Nevertheless, further increments in μ lowers V_{data} due to the accumulation of handoffs that occur, which leads to a lower data rate between the CAV and BS. It is important to note that the objective function in **P2** is proportional to the speed, therefore, our goal is to maximize the speed while satisfying $V_{\max}, V_{\text{safe}}$, and $V_{\text{data}}(\mu)$. □

Fig. 3.2 depicts the relation between μ and v. At first, an increase in the active BS density improves the data rate; thus the speed (as well as traffic flow) improves. Nonetheless, the unimodal shape of V_{data} comes from the fact that when the active BS density μ further increases, this results in more frequent handoffs which reduces data rate. To showcase the relation between μ and v further, Fig. 3.2 depicts two scenarios with different CAV processing times τ which directly impact V_{safe} and $V_{\min} = \min\{V_{\max}, V_{\text{safe}}\}$. The discussions are as follows:

- **Scenario 1 ($\tau = 1.5 \times 10^{-4}$ sec)**: As seen in the top plot of Fig. 3.2, $V_{\min}$ is above the peak of the V_{data} curve, and $V_{\min}$ does not intersect with V_{data}.

Therefore, $V_{\max}$ and V_{safe} values are higher compared to the speed required to support data rate, i.e., V_{data}, and the maximum speed that a CAV can have along with satisfying data rate requirements is the peak of V_{data}. The peak of V_{data} requires the optimal active BS density μ^*, where $\mu_{\text{data}} \leq \mu^* \leq \mu_{\max}$ that in turn maximizes the traffic flow while satisfying the data rate requirement. This optimal active BS density μ^* also holds if $V_{\min}$ becomes equal to the peak of V_{data} (i.e. $V_{\min}$ lies on top of the peak of the V_{data} curve).

- **Scenario 2 ($\tau = 4 \times 10^{-4}$ sec):** As seen in the bottom plot of Fig. 3.2, $V_{\min}$ lies below the peak of V_{data} and intersects with V_{data} at two points. This means that the maximum speed (and in turn the traffic flow) can be achieved only at those two intersections while satisfying $V_{\max}$, V_{safe} as well as data rate. In contrast, any active BS density is optimal between the two intersections since the data rate connectivity holds; however, the optimal active BS density should also satisfy **C4**, i.e., $\mu_{\text{data}} \leq \mu^* \leq \mu_{\max}$. The vertical lines are the minimum required active BS density given by μ_{data} in (3.10) and maximum active BS density $\mu_{\max}$, respectively. Thus, any value of μ can be selected between the two intersections, where $\mu_{\text{data}} \leq \mu^* \leq \mu_{\max}$.

Since $V_{\min}$ depends on variables such as crash probability ϵ and processing time τ, the values for these two variables affect $V_{\min}$. For example, if the CAVs take a longer time τ to process data for decision-making or if the crash probability ϵ is high, V_{safe} reduces in order to maintain a safety distance with other CAVs to avoid collisions.

In order to find a closed form solution for the optimal density of BSs μ^*, first we maximize the traffic flow by taking the derivative of equation (3.8) with respect to μ

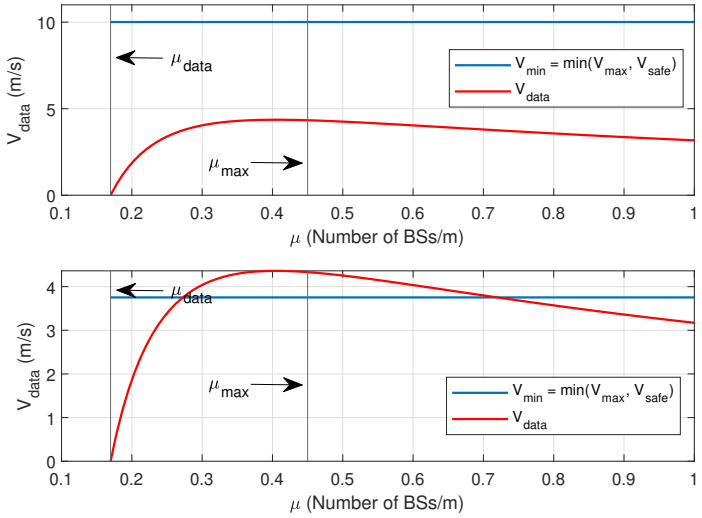

Figure 3.2: Graphical demonstration of the constraints and V_{data} as a function of μ. $R_{\text{th}} = 1$ Gbps, $\alpha = 3$, $\epsilon_1 = 0.15\%$.

and numerically solve the following to get $\hat{\mu}$, i.e.,

$$\hat{\mu} \implies \frac{\partial V_{\text{data}}(\mu)}{\partial \mu} = 0 \tag{3.14}$$

where

$$\frac{\partial V_{\text{data}}(\mu)}{\partial \mu} = \frac{1}{\bar{h}_d \mu^2} \left(\frac{R_{\text{th}} \left(\bar{\gamma} \alpha (2\mu)^{\alpha} + z \log_2(z) \right)}{W_{\text{c}} z \log_2^2(z)} - 1 \right) \tag{3.15}$$

where $z = 1 + \bar{\gamma}(2\mu)^{\alpha}$. Then, considering constraint **C4**, the optimal μ^* is given as:

$$\mu^* = \begin{cases} \hat{\mu} & \mu_{\text{data}} \leq \hat{\mu} \leq \mu_{\text{max}} \\ \mu_{\text{max}} & \hat{\mu} \geq \mu_{\text{max}} \end{cases} \tag{3.16}$$

Note that if $\hat{\mu} \leq \mu_{\text{data}}$ then the problem becomes infeasible as it violates **C4**,

In scenarios with a large density of BSs, the SNR at the receiver remains sufficiently high. For such scenarios, we derive a closed-form expression for the optimal active BS density as shown in the following Lemma.

Lemma 2. *Substituting* $z = 1 + \bar{\gamma}(2\mu)^{\alpha}$ *with* $\hat{z} = \bar{\gamma}(2\mu)^{\alpha}$*, i.e., approximating 1 + SNR* $\approx$ *SNR in the data rate equation* (3.8)*, the closed form solution of* μ^* *can be given as:*

$$\hat{\mu} = \frac{1}{2\bar{\gamma}^{1/\alpha}} \left(2^{((R_{\text{th}})^{1/2}(R_{\text{th}}+4W_c R_{\text{th}}\alpha)^{1/2}+R_{\text{th}}))(2W_c)^{-1}}\right)^{1/\alpha}. \tag{3.17}$$

Finally, μ^* *can be obtained by substituting* (3.17) *in* (3.16)*.*

Proof. Considering high SNR regime, we can rewrite (3.8) as:

$$\tilde{V}_{\text{data}}(\mu) = \frac{1}{\bar{h}_d \mu} \left(1 - \frac{R_{\text{th}}}{W_c \log_2(\hat{z})}\right), \tag{3.18}$$

According to the first order condition [29], taking the derivative of (3.18) with respect to μ and equating to zero, we have the following:

$$\frac{\partial \tilde{V}_{\text{data}}(\mu)}{\partial \mu} = \frac{R_{\text{th}}\alpha + \log_2(\hat{z})(R_{\text{th}} - W_{\text{c}} \log_2(\hat{z}))}{\bar{h}_{\text{d}} \mu^2 \log_2^2(\hat{z})} = 0, \tag{3.19}$$

Finally, solving for μ, we present the closed form solution for $\hat{\mu}$ as given in **Lemma 2**. The second order condition shows concavity of $\tilde{V}_{\text{data}}$ w.r.t. μ. □

Remark: The maximum traffic flow can be computed by substituting (3.16) into the optimal speed expression given by (3.12) in **Lemma 1**, and then substituting the optimal speed in the objective function of **P2**, i.e.,

$$Q = \min\{V_{\max}, V_{\text{safe}}, V_{\text{data}}(\mu^*)\} \lambda e^{\lambda l} \Gamma(0, \lambda l) \tag{3.20}$$

3.3 Microscopic Traffic Flow Maximization

The macroscopic traffic flow model is useful to analyze the traffic flow for a stream of CAVs, however it lacks the interaction between individual CAVs and assumes many assumptions which could have implications on the traffic flow since the worst-case SNR was assumed. In this section, we analyze the correlation of vehicular connectivity and road traffic flow from a microscopic perspective. We consider a CAV traffic flow based on the well-known Pipe's car-following model [16]. The original Pipe's model considers a *safe headway* between a pair of CAVs: the leader and CAV, with the former driving in front of the latter. If the spacing is larger than the safe headway, the CAV accelerates to reduce the spacing and keep the safe headway with the leader. In contrast, if the spacing is less than the safe headway, the CAV decelerates to increase the spacing and keep the safe headway with the leader.

3.3.1 Pipe's Model with Reference Speed

We use a similar approach as Pipe's model but consider speed instead of the safe headway to derive motion dynamics. We consider v^{ref} as the *reference speed*, which all CAVs seek to maintain. When the CAV's speed drops below the reference speed, it accelerates to reach and maintain the reference speed. In contrast, if the CAV's speed surpasses the reference speed, it decelerates to reach and maintain the reference

speed. Thus, the speed of each CAV evolve as follows:

$$v(t+\Delta t) = \begin{cases} \max\{v(t) - d_a\tau, 0\} & v(t) > v^{\text{ref}}(t+\Delta t) \\ v(t) & v(t) = v^{\text{ref}}(t+\Delta t) \\ \min\{v(t) + a\tau, V_{\max}\} & v(t) < v^{\text{ref}}(t+\Delta t), \end{cases} \tag{3.21}$$

where d_a and a are the maximum deceleration and acceleration, respectively. This formulation forces vehicles to accelerate if their speed is less than the reference speed, and decelerate if their speed is larger than the reference speed. The ultimate goal is to maintain the reference speed. Note that $v^{\text{ref}}(t)$ and $v(t)$ are the reference speed and the actual speed of an CAV at time t, respectively. Also, d_a, a, and $V_{\max}$ represent the deceleration, acceleration, and maximum speed of CAVs, respectively.

At a given time instant $t + \Delta t$, the distance ($s_{i,i+1}$) between successive CAVs i and $i+1$ is given as follows:

$$s_{i,i+1}(t+\Delta t) = s_{i,i+1}(t) + (v_{i+1}(t) - v_i(t))\Delta t \tag{3.22}$$

In what follows, we formulate the microscopic traffic flow maximization problem subject to network and transportation constraints considering a given CAV density k defined as the number of CAVs (N) per unit length of the road (L).

3.3.2 Problem Formulation

In this subsection, we present the microscopic traffic flow maximization at a particular time t, taking into account the speed of each CAV where $\mathbf{v}(t) = \{v_1(t), v_2(t), \ldots, v_N(t)\}$ and $\mathcal{N} = \{1, 2, \ldots, N\}$ is the set of all CAVs. The traffic flow maximization problem,

consistent with the proposed macroscopic model, can then be presented as follows:

$$
\begin{aligned}
(\mathbf{P3}) \quad & \max_{\mathbf{v},\mu} \qquad Q = \frac{k}{N}\sum_{i=1}^{N} v_i(t+\Delta t) \\
\text{s.t.}(\mathbf{C1}) \quad & v_i(t+\Delta t) \leq \frac{s_{i,i+1}(t)-l}{\tau}, \forall i \in \mathcal{N} \\
(\mathbf{C2}) \quad & v_i(t+\Delta t) \leq \frac{1}{\bar{h}_d \mu}\left(1 - \frac{R_{\text{th}}}{W_c \log_2\left(\hat{y}(t)\right)}\right), \forall i \in \mathcal{N} \\
(\mathbf{C3}) \quad & 0 \leq v_i(t+\Delta t) \leq V_{\max}, \forall i \in \mathcal{N} \\
(\mathbf{C4}) \quad & \mu_{\text{data}} \leq \mu \leq \mu_{\max}
\end{aligned}
$$

where $k = N/L$ and $\hat{y}(t) = 1 + \bar{\gamma}(d_{i,j}(t))^{-\alpha}$. **C1** considers the update in speed with safety distance based on the current spacing between two CAVs, $s_{i,i+1}(t)$, and **C2** considers the update in speed with mobility-aware data rate based on the current distance between a CAV and its closest BS, $d_{i,j}(t)$.

In order to conduct microscopic traffic flow analysis with the network constraints, we alter equations (3.7) and (3.8) as in **C1** and **C2**, respectively, to fit the microscopic model. More specifically, we consider the real-time distance between a CAV and BS (as compared to worst distance in the macroscopic model), as well as the spacing between every leader-follower pair of CAVs. The equations are as follows:

$$
v_i(t+\Delta t) \leq \frac{s_{i,i+1}(t)-l}{\tau} = V_{i,\text{safe}}(t+\Delta t), \tag{3.23}
$$

where $s_{i,i+1}(t)$ is the distance between the the leader and CAV i at time t.

$$v_i(t+\Delta t) \leq \frac{1}{\bar{h}_d \mu}\left(1 - \frac{R_{\text{th}}}{W_c \log_2\left(1+\bar{\gamma} d_{i,j}^{-\alpha}(t)\right)}\right)$$
$$= V_{i,\text{data}}(t+\Delta t). \tag{3.24}$$

where $d_{i,j}$ is the distance between CAV i and its closest BS j at time t, and $\bar{\gamma} = \frac{\gamma_R P_j^{\text{tx}} \chi_{i,j}}{N_R}$. We consider a Rayleigh transmission fading channel $\chi_{i,j}$ which is exponentially distributed.

Since the network planning and deployment is a long-term optimization problem, in the microscopic model, we apply the optimal active BS density solution given by equation (3.16) which stems from the solution of **P2** in the macroscopic model. Therefore, for the deployment of BSs in the microscopic model, we use μ^* (3.16). Therefore, given μ^* from the macroscopic model, we can re-write **P3** as follows:

$$\begin{aligned}
(\mathbf{P4}) \quad & \max_{\mathbf{v}} \qquad Q = \frac{1}{L}\sum_{i=1}^{N} v_i(t+\Delta t) \\
\text{s.t.}(\mathbf{C1}) \quad & v_i(t+\Delta t) \leq \frac{s_{i,i+1}(t) - l}{\tau}, \forall i \in \mathcal{N} \\
(\mathbf{C2}) \quad & v_i(t+\Delta t) \leq \frac{1}{\bar{h}_d \mu}\left(1 - \frac{R_{\text{th}}}{W_c \log_2\left(\hat{y}(t)\right)}\right), \forall i \in \mathcal{N} \\
(\mathbf{C3}) \quad & 0 \leq v_i(t+\Delta t) \leq V_{\max}, \forall i \in \mathcal{N}
\end{aligned}$$

Since the objective function increases monotonically with v, the optimal speed for an individual vehicle i at time t lies at the boundary of the constraints **C1, C2, C3**, i.e.,

$$v_i^*(t+\Delta t) = \min\{V_{\max}, V_{i,\text{safe}}(t+\Delta t), V_{i,\text{data}}(t+\Delta t)\}, \tag{3.25}$$

where (3.25) represents the optimal speed of CAV i at any given time to maximize the traffic flow. Furthermore, since we do not consider acceleration in (3.25) for consistency with the macroscopic model, we apply the optimal speed to Pipe's model (3.21) for simulation purposes by replacing $v^{\text{ref}}(t+\Delta t)$ with $v_i^*(t+\Delta t)$ as follows.

$$v_i(t+\Delta t) = \begin{cases} \max\{v_i(t) - d_a\tau, 0\} & v_i(t) > v_i^*(t+\Delta t) \\ v_i(t) & v_i(t) = v_i^*(t+\Delta t) \\ \min\{v_i(t) + a\tau, V_{\max}\} & v_i(t) < v_i^*(t+\Delta t). \end{cases} \tag{3.26}$$

In the following, we present steps to optimize the speed of each CAV at each time instant, with updates to the speed and spacing between CAVs given by the Pipe's model in equations (3.22) and (3.26), respectively.

3.3.3 Optimizing the CAVs' Speed and Computing the Average Traffic Flow

we initialize the optimal active BS density from equation (3.16) by considering the maximum data rate requirement R_{th} of all the CAVs. We store the x-coordinate of each CAV on the road at every time step in a vector $\mathbf{x}$, calculate the distances between each CAV using (3.22), and the CAV locations are then updated every T_f, which represents the resolution of the simulation. The steps to optimize the CAVs' speed at every time step t and compute the average traffic flow are detailed as follows:

1. Initialize the x-coordinates and distances between CAVs randomly. Calculate μ using equation (3.16) and initialize CAVs' speeds as $V_{\max}$.

2. Calculate $V_{i,\text{safe}}(t+\Delta t)$ using equation (3.23).

3. Calculate $V_{i,\text{data}}(t + \Delta t)$ using equation (3.24).

4. Calculate $v_i^*(t + \Delta t)$ using equation (3.25).

5. Calculate $v_i(t + \Delta t)$ using equation (3.26)

6. Update CAV x-coordinates and CAV to BS distances $d_{i,j}(t)$ after every time duration of T_f.

7. Calculate $s_{i,i+1}(t + \Delta t)$ using equation (3.22).

8. Repeat steps 2-6 for each CAV.

9. Calculate the average traffic flow using the objective function in **P4**.

10. Repeat steps 2-9 up to a time limit.

3.4 Numerical Results and Discussions

In this section, we validate the accuracy of the derived expressions through computer simulations, Also, we perform sensitivity analysis on key parameters to assess the inter dependency of the traffic flow, CAVs maximum achievable speed, and optimal active BS density. We initially present the macroscopic and microscopic results separately in the following subsections and then compare results for both macroscopic and microscopic respectively.

3.4.1 Macroscopic Model Results

3.4.1.1 System Parameters

Unless stated otherwise, the values of the system parameters [24] used in the following figures are listed herein. $V_{\max} = 30$ m/s, $\mu_{\max} = 0.45$ BSs/m, $h_d = 1$ s/handoff,

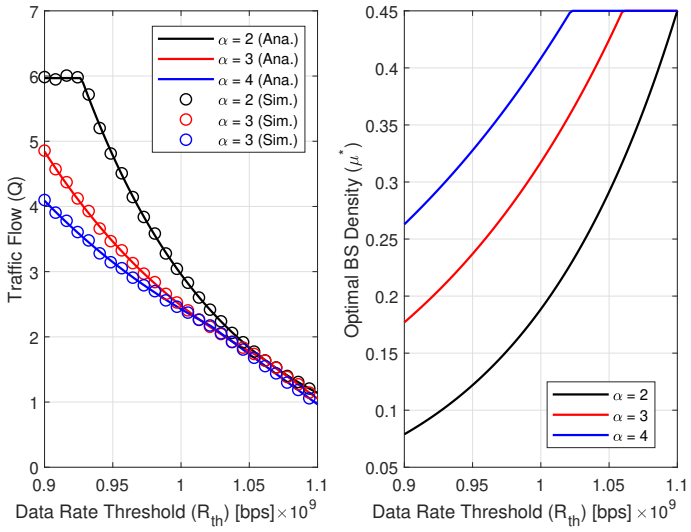

Figure 3.3: Traffic flow Q as a function of R_{th} with analytical and simulation results (Left) and optimal density μ^* as a function of R_{th} (Right) with varying path-loss exponents α.

$R_{\text{th}} = 1$ Gbps, $W_c = 40$ MHz, $G_{\text{tx}} = 1$ dB, $G_{\text{rx}} = 1$ dB, $c = 3 \times 10^8$ m/s, $f_R = 2.1$ GHz, $N_R = 1.507 \times 10^{-13}$ W/m^2, $P_j^{\text{tx}} = 1$ W, $\alpha = 3$, $l = 1$ m, $\lambda = 1$ m, $\epsilon = 0.15\%$, $\tau = 1.5 \times 10^{-4}$ sec.

3.4.1.2 Impact of Wireless Environment on Road-Traffic Flow

Fig. 3.3 confirms the accuracy of the derived closed-form traffic flow expression given in equation (3.20) through Monte-Carlo simulations. Also, Fig. 3.3 depicts the impact of CAV's data rate requirement R_{th} on the traffic flow Q considering a variety of path-loss exponents (which are a representative of wireless channel environment) α. As seen in the left-hand side of Fig. 3.3, as R_{th} increases, the traffic flow Q decreases. This is because the CAVs need to lower their speed to reduce handoffs and in turn achieve the required data rate, that naturally reduces the traffic flow. Moreover, it is critical to note that for lower path-loss exponents such as $\alpha = 2$ (which implies

free-space path-loss), higher traffic flow is achieved compared to higher path-loss exponent $\alpha = 4$ (which implies outdoor environments). Physically this means that environments with lower path-loss achieve higher data rates and traffic flow, whereas environments with higher path-loss achieve reduced data rates and traffic flow.

On the other hand, Fig. 3 depicts the optimal active BS density as a function of the CAV data rate requirement R_{th}. As shown on the right-hand side of Fig. 3.3, for lower path-loss exponent ($\alpha = 2$) which implies free-space path-loss, optimal density of BSs is lower due to better transmission channels compared to $\alpha = 4$ (which implies outdoor environment with higher propagation losses). However, as R_{th} increases, the optimal active BS density also increases. At this point, it is noteworthy that while the increase in μ is advantageous in terms of increasing SNR and data rate, this increase in μ also increases handoffs which reduces speed and traffic flow (as is also evident from equation (3.8)).

3.4.1.3 Impact of the Density of BSs on Road-Traffic Flow

Fig. 3.4 and depicts the impact of the density of BSs μ on traffic flow Q considering various CAV processing times τ. As μ increases, Q increases up to a certain point and begins to decrease due to an increase of handoffs as can be observed from equation (3.8). We observe that when the processing time τ is smaller, V_{safe} increases as can be observed from equation (3.7). Physically, this means that CAVs take a shorter amount of time in decision making to change their speeds so they are able to achieve higher speeds. Alternatively, when the processing time τ is larger, V_{safe} decreases, which means the CAVs take a longer time in decision making which results in lower speeds for collision avoidance. Furthermore, since V_{data} depends on μ, we observe a

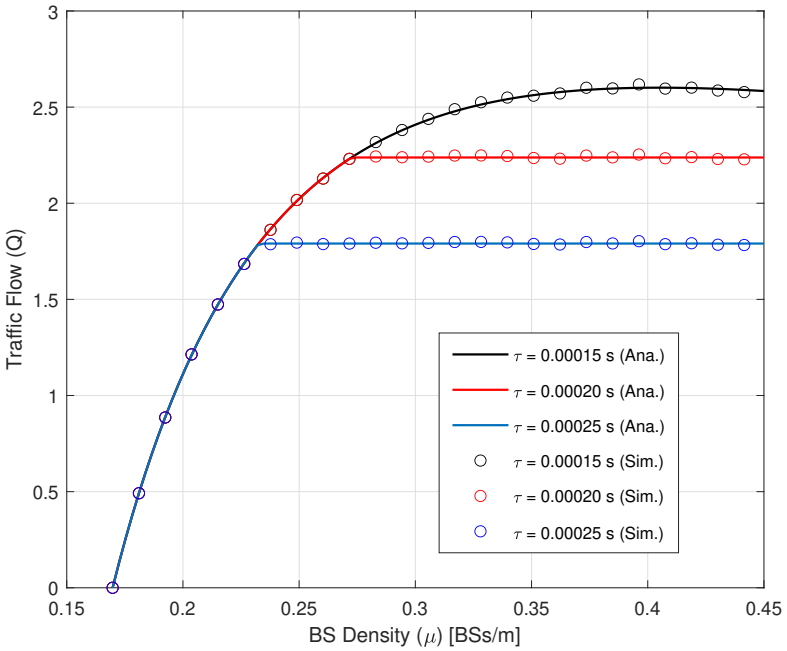

Figure 3.4: Traffic flow Q as a function of μ with analytical and simulation results with varying processing times τ.

similar pattern as in Fig. 3.2 where V_{data} increases as μ increases, and the optimal speed given in equation (3.12) follows V_{data} in the range where $V_{\text{safe}} > V_{\text{data}}$ up to a certain value of μ. However, when μ becomes large up to a certain point, we observe that $V_{\text{safe}} < V_{\text{data}}$, and due to equation (3.12), the optimal speed follows V_{safe} which is constant with respect to μ.

3.4.2 Pipe's Model Simulation Results

3.4.2.1 System Parameters

Unless stated otherwise, the values of the system parameters [24] used in the following figures are listed herein. $N = 10$ CAVs, $V_{\max} = 30$ m/s, $\mu_{\max} = 0.45$ BSs/m, $h_d = 1$ s/handoff, $W_c = 40$ MHz, $G_{\text{tx}} = 1$ dB, $G_{\text{rx}} = 1$dB, $c = 3 \times 10^8$ m/s, $f_R = 2.1$

GHz, $N_R = 1.507 \times 10^{-13}$ W/m^2, $P_j^{\text{tx}} = 1$ W, $\alpha = 3$, $l = 1$ m, $\tau = 0.4$ sec, CAV starting speeds $\mathbf{v}(1) = 12.5$ m/s, and the length of the road is 100 m. Furthermore, we consider various data rate thresholds R_{th} for different CAVs. Specifically, half of the CAVs have $R_{\text{th}} = 0.6$ Gbps and the other half have $R_{\text{th}} = 0.8$ Gbps. By using (3.16), μ^* is calculated using the maximum R_{th} value.

3.4.2.2 Pipe's Model Simulation with Network Constraints

Figs. 3.5 and 3.6 depict the change in CAV distance and speed over time considering optimal active BS density (μ^*) and a minimum active BS density (μ_{data}), respectively, to ensure connectivity as detailed in the CAV speed optimization steps in section 3.3.3. The figures show the distances and speeds of the individual CAVs denoted by the faded curves as well as the average distance and speed denoted by the black curves.

Fig. 3.5 considers the optimal number of BSs calculated from equation (3.16). As seen in the distance plot of figure, the CAVs are consistently moving and do not come to full stops, while also maintaining a safety distance. When a CAV comes into close contact with another CAV, it slows down its speed enough to avoid a collision, but at the same time, it does not impede traffic compared to Fig. 3.6 where the CAVs come to a complete stop at times because of fewer deployed BSs. Furthermore, we observe that the CAVs constantly change their speeds, which is due to the network connectivity constraints presented in **P4** which optimizes individual CAV speeds based on safety speeds and data rates.

In addition, Fig. 3.6 depicts the model with the minimum number of required BSs calculated from equation (3.10). In other words, we performed the same simulation

as Fig. 3.5 with less BSs, but still ensures the feasibility requirement by meeting the constraint $\mu_{\text{data}} < \mu < \mu_{\max}$. As seen in the figure, the CAVs tend to come to complete stops before accelerating again, which is evident in the speed plot where the CAV speeds reach zero.

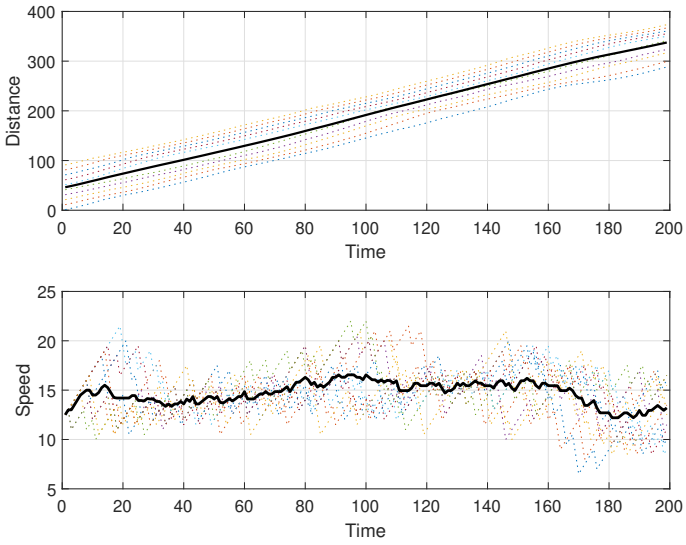

Figure 3.5: Pipe's Model with Network Connectivity Constraints: $\mu = \mu^*$.

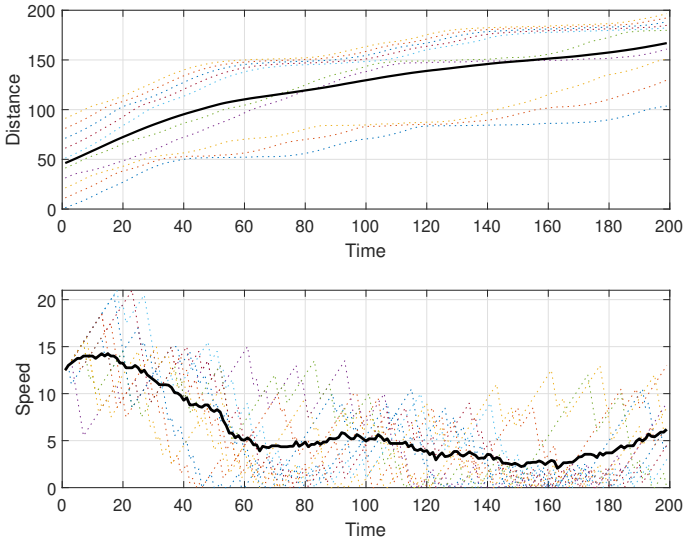

Figure 3.6: Pipe's Model with Network Connectivity Constraints: $\mu = \mu_{\text{data}}$.

3.4.3 Macroscopic and Microscopic Traffic Flow Comparison

3.4.3.1 Impact of the CAVs Spacing on Road-Traffic Flow

Fig. 3.7 depicts the impact of the average CAV density λ on the CAV speed v (top) and traffic flow Q (bottom) under various R_{th} values for both the macroscopic and microscopic traffic flow models. We note that higher CAV density limits the CAVs from moving faster; thus the required speed threshold to avoid collision reduces V_{safe}, while V_{data} remains constant w.r.t λ. On the other hand, relative to the macroscopic traffic flow curves, as the λ increases, Q increases up to a certain point before decreasing. The initial increase in traffic flow is due to the increase in average traffic density which is the reciprocal of λ. However, as soon as we approach the intersection of V_{data} and V_{safe}, the traffic flow starts reducing due to reduced density of CAVs on the road which results in the reduction of V_{safe}. Furthermore, as described in Fig. 3.7, satisfying higher data rate requirements requires reduced speeds thus resulting in lower

traffic flow. On the other hand, the microscopic average traffic flow curves (as presented in the objective function of **P4** are synonymous to the macroscopic traffic flow curves, where we show the impact of various data rate thresholds R_{th} while using the same system parameters detailed in the macroscopic results section. As seen in the Fig. 3.7, the average traffic flow is not only higher in comparison to the macroscopic model, but can also support higher data rate thresholds without severely degrading the traffic flow. This is the implication when the spacing between individual CAVs are considered and are not assumed to all be the same like in the macroscopic model. Therefore, better traffic flow can be achieved and higher data rates can be supported with microscopic analysis and optimization.

3.4.3.2 Impact of the Density of BSs on Road-Traffic Flow

Fig. 3.8 depicts the impact of the active BS density μ on traffic flow Q for both the macroscopic and microscopic car following models. We observe that higher data rate requirements results in lower traffic flow since they need to reduce their speed to meet the data rate requirements. Similarly, we observe that the minimum active BS density required for the CAVs to operate in the environment given by μ_{data} (3.10) increases for larger data rate requirements. Therefore, this allows for system designers to select the maximum required active BS density based on the data rate requirements of different CAVs on the road with various data rate thresholds. On the other hand, the microscopic traffic flow curves follow a similar trend to the macroscopic traffic flow results, however the microscopic model achieves better traffic flow compared to the macroscopic model.

Therefore, we conclude that when analyzing the average traffic flow with respect

to the active BS density, the macroscopic model achieves relatively accurate results and can easily be simulated, whereas the microscopic model achieves better results when analyzing the traffic flow with respect to the CAV density on the road but is more complicated to simulate than macroscopic traffic flow.

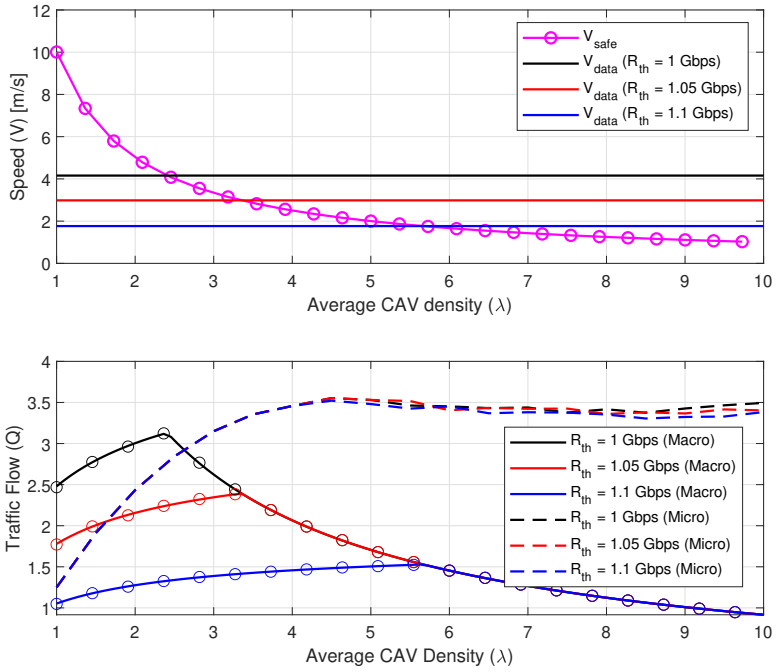

Figure 3.7: Speed as a function of average CAV density λ (top) Macroscopic and Microscopic traffic flow Q as a function of λ (bottom) with analytical and simulation results and varying data rate thresholds R_{th}.

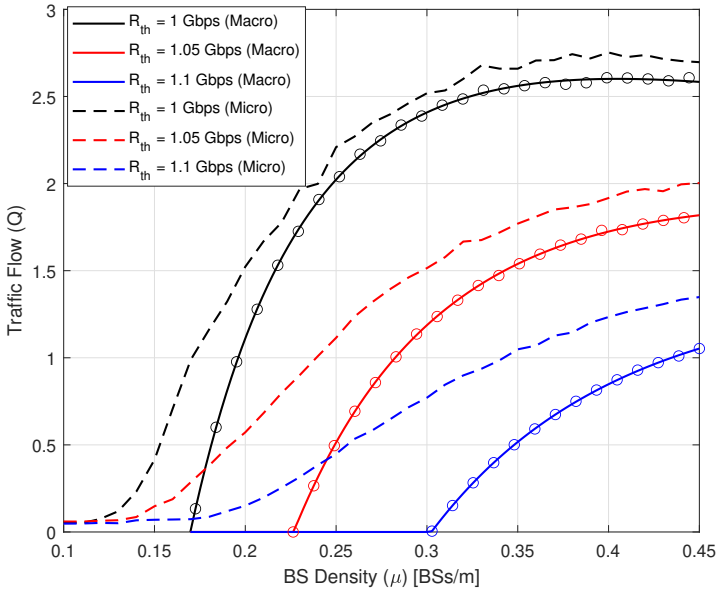

Figure 3.8: Macroscopic and microscopic traffic flow Q as a function of μ with analytical and simulation results with varying data rate thresholds R_{th}.

3.5 Summary

In this chapter, we present a framework for V2I communication of CAVs where we optimize speeds and BS densities through transportation traffic flow constraints and network connectivity constraints to maximize traffic flow. In the proposed framework, we consider a macroscopic traffic flow model to derive the optimal speed and active BS density, and verify the results through computer simulations where we demonstrate the trade-off between achievable wireless data rates and CAV traffic flow. Finally, we simulate the microscopic traffic flow model where we incorporate the aforementioned network connectivity constraints to optimize individual CAV speeds, and the simulations show improvement in traffic flow with respect to CAV density in comparison to the macroscopic model. Although the microscopic model achieves better traffic flow

when analyzing CAV density, the macroscopic model is crucial to determine optimal BS densities in long-term decision problems for BS deployment.

Chapter 4

V2I Constrained Macroscopic Traffic Flow Maximization with Interference

4.1 Motivation and Contribution

This chapter provides a comprehensive framework to assess the effect of interference and channel fading in the telecommunication model and how it affects the optimal traffic flow. Dense BS deployment is known to cause unnecessary interference which can negatively impact the SINR and data rate [51]. In the previous chapter, we assumed there was no interference in the system model, however in real-world scenarios, wireless communications are subject to interference from neighbouring BSs and the surrounding environment, and is important to consider when analyzing V2I communications for CAV traffic flow. To this end, the contributions in this chapter can be summarized as follows:

- We characterize macroscopic traffic flow by considering log-normal distribution of the spacing between CAVs. Then, we derive novel and tractable closed-form expressions for the probability density function (PDF) and cumulative

density function (CDF) of signal-to-interference-plus-noise ratio (SINR), HO-aware rate outage probability and ergodic capacity in a large-scale network with interference. The derived expressions capture the network parameters such as height of the BSs, safety distance of BSs from the road, interference from neighboring BSs, and channel fading.

- We develop a novel optimization framework to jointly optimize the active BS density and speed of CAVs to maximize the CAVs' traffic flow with collision avoidance and minimum HO-aware data rate constraints.

- Our numerical results confirm the accuracy of the derived expressions and extract useful insights related to dynamics of active BS density, CAV minimum data rate requirements, average CAV speed, BS heights and safety distances, etc.

4.2 System Model and Performance Metrics

We consider a road of length L_R on which N_c CAVs travel. We consider N BSs are deployed alongside the road at a certain distance d_{safe} with a density defined as the number of BSs deployed per unit distance, i.e., $\mu = N/L_R$. The distance between BSs is $1/\mu$ as shown in Fig. 4.1. The CAVs' density k on the road is defined as the number of CAVs per unit distance, and the CAVs' speed is v. According to macroscopic traffic flow theory, the flow of vehicles is defined as $q = kv$ vehicles per unit time [52]. Note that k is inversely proportional to s, i.e., $k = 1/s$ and s is the spacing between neighboring vehicles. Given the PDF of the density of vehicles k on

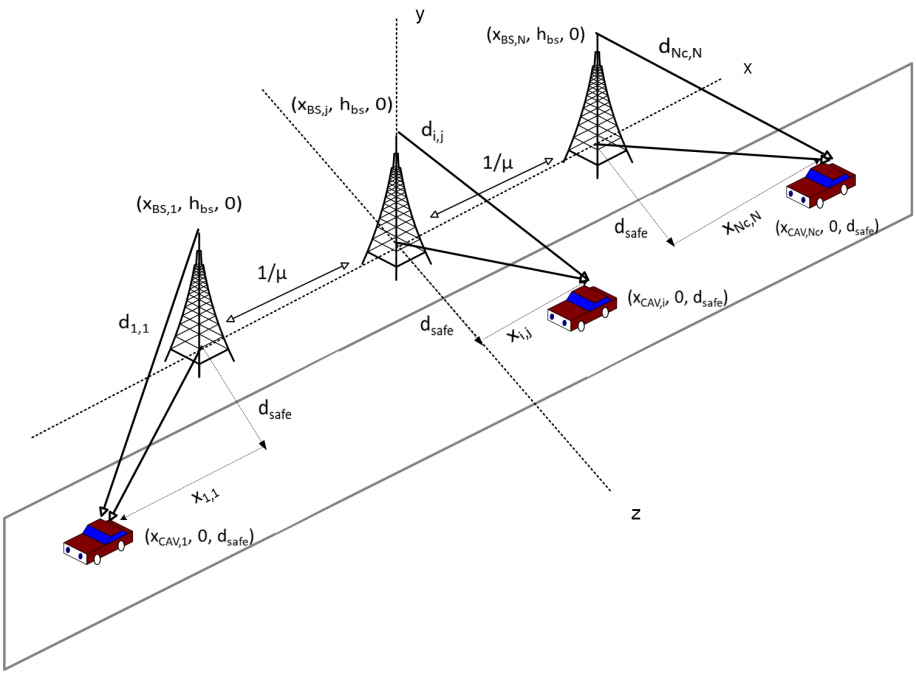

Figure 4.1: Graphical illustration of the V2I communication model for CAVs.

the road $f_K(k)$, the traffic flow can be defined as follows:

$$Q = \int_0^\infty kv f_K(k) \mathrm{d}k. \tag{4.1}$$

In this chapter, we model the inter-vehicle spacing s with a log-normal distribution. This model has been proven to be accurate for daytime hours through various empirical studies [53]. The research works observed the traffic flow behaviour during different times of the day, and proved that the inter-vehicle spacing distribution is log-normally distributed during day-time hours (i.e., moderate traffic). Therefore, we consider the inter-vehicle spacing s to be log-normally distributed during day-time

hours with PDF given as:

$$f_S(s) = \frac{1}{s\sigma_{\mathrm{LN}}\sqrt{2\pi}} \exp\left(-\frac{(\ln(s) - \mu_{\mathrm{LN}})^2}{2\sigma_{\mathrm{LN}}^2}\right),$$

where μ_{LN} and σ_{LN} are the logarithmic average and scatter parameters of log-normal distribution, respectively, and erf$(\cdot)$ is the error function. Therefore, (4.1) can be rewritten as follows:

$$Q = \int_0^{\infty} \frac{1}{s} v f_S(s) \mathrm{d}s = v \exp\left(\frac{\sigma_{\mathrm{LN}}^2 - 2\mu_{\mathrm{LN}}}{2}\right). \tag{4.2}$$

Each CAV is assumed to be connected to a single nearest BS at any given time. Considering the distance-based path-loss and short-term multi-path fading at the transmission channel, the received signal power at a given CAV i from a given BS j in the downlink can be modeled as follows:

$$S_{i,j} = G_R^{\mathrm{tx}} G_R^{\mathrm{rx}} \left(\frac{c}{4\pi f_R}\right)^2 \frac{P_j^{\mathrm{tx}}}{d_{i,j}^{\alpha}} \chi_{i,j} = \gamma_R P_j^{\mathrm{tx}} d_{i,j}^{-\alpha} \chi_{i,j}, \tag{4.3}$$

The signal-to-interference-plus noise ratio (SINR) received at a i-th CAV from j-th BS can thus be modeled as follows:

$$\mathrm{SINR}_{i,j} = \frac{S_{i,j}}{N_R + I_i} = \frac{\gamma_R P_j^{\mathrm{tx}} d_{i,j}^{-\alpha} \chi_{i,j}}{N_R + I_i}, \tag{4.4}$$

where G_R^{tx} and G_R^{rx} represent the transmitting and receiving antenna gains, respectively, P_j^{tx} represents the transmit power of the BS j, $\chi_{i,j}$ represents the short-term channel fading of BS j modeled with Rayleigh distribution, c and f_R represent the

speed of an electromagnetic wave and RF carrier frequency, respectively, $d_{i,j}$ represents the distance between the j-th BS and i-th CAV, and α represents the path-loss exponent. Furthermore, N_R is the thermal noise power at the receiver and $I_i = \sum_{k \neq j} P_k^{\text{tx}} \gamma_R d_{i,k}^{-\alpha} \chi_{i,k}$ is the cumulative interference at the i-th CAV from the interfering BSs, where $\gamma_R = G_R^{\text{tx}} G_R^{\text{rx}} (c/4\pi f_R)^2$, $d_{i,k}$ represents the distance between the i-th CAV and k-th interfering BS, and $\chi_{i,k}$ is the power of fading from the k-th interfering BS to the CAV.

Furthermore, as detailed in Fig. 1, the distance between a CAV i and BS j can be calculated using their respective coordinates as $d_{i,j} = \sqrt{x_{i,j}^2 + h_{\text{bs}}^2 + d_{\text{safe}}^2}$, where h_{bs} represents the height of the BSs, d_{safe} represents the safety distance from the CAV on the road to the BS, and $x_{i,j}$ is the distance parallel to the road with respect to the location of the CAV on the road to the BS. Subsequently, given the Shannon-Hartley theorem for infinite block-length regime [25], the data rate without mobility between a BS and CAV can be defined as $R_{i,j} = W \log_2(1 + \text{SINR}_{i,j})$ where W represents the bandwidth of the channel.

As CAVs drive along the road, HOs between different BSs occur, and due to HO delays and failures, an increase in the rate of HOs can negatively impact the CAV data rate. Therefore, we incorporate the effect of these HOs through the HO-related cost. HO cost is proportional to the HO delay (h_d) measured in seconds per HO, and HO rate (H) measured in number of HOs per second [31], i.e., $H_c = h_d \times H$. Since we assume nearest BS association for CAVs, we define H as the *number of cell boundaries a CAV crosses per second*, where a cell boundary is the coverage range of a BS. Note that the number of boundaries per unit distance are the same as the active BS density μ. Furthermore, by using the speed of CAVs v, we can calculate

the number of boundaries covered by a CAV per second as $H = \mu v$. Subsequently, we model the HO-aware data rate [30] as follows:

$$M_{i,j} = R_{i,j}(1 - H_{c,\max}) = R_{i,j}\left(1 - h_d \frac{\mu v_i}{\mu_{\max} V_{\max}}\right), \tag{4.5}$$

where $H_{c,\max} = h_d \frac{H}{\mu_{\max} V_{\max}} = h_d \frac{\mu v}{\mu_{\max} V_{\max}}$ is the normalized HO cost in equation (4.5) to ensure $0 \leq H_{c,\max} < 1$, $\mu_{\max}$ is the maximum regulated active BS density, and $V_{\max}$ is the maximum regulated speed of the CAVs. Finally, a stable CAV connection with the nearest BS requires a minimum HO-aware data rate R_{th} which ensures that every CAV achieves the required QoS.

4.3 HO-Aware Rate Outage Probability Analysis

In this section, we derive novel closed-form expressions for the PDF and CDF of SINR, HO-aware rate outage probability, as well as the ergodic HO-aware data rate.

The HO-aware rate outage probability P_{out} is defined as:

$$P_{\text{out}} = \Pr\left(M_{i,j} \leq R_{\text{th}}\right) = \Pr\left(Z = \frac{S_{i,j}}{N_R + I_i} \leq \gamma_{\text{th}}\right), \tag{4.6}$$

where γ_{th} is the desired SINR threshold given as $\gamma_{\text{th}} = 2^{\frac{R_{\text{th}}}{W(1-H_{c,\max})}}$ and $H_{c,\max} = h_d \frac{\mu v}{\mu_{\max} V_{\max}}$. The outage expression can then be derived as shown in the following lemma.

Lemma 3 (HO-aware Rate Outage Probability)**.** *Given the PDF and CDF of SINR*

of ith CAV, the closed-form outage expressions can be given as follows:

$$P_{\text{out}} = 1 - \sum_{k=1,k\neq j}^{N} \frac{a_{i,j} e^{\frac{\lambda N_R}{b_{i,k}}}}{b_{i,k}\gamma_{\text{th}} + a_{i,j}} \prod_{l=1,l\neq k} \frac{b_{i,k}}{b_{i,k} - b_{i,l}}. \tag{4.7}$$

Proof. To derive the SINR outage, we first calculate the PDF and CDF of SINR. In the sequel, we first determine the PDF and CDF of $S_{i,j}$ and I_i. The random variable $S_{i,j}$ is a scaled exponential random variable, i.e., $S_{i,j} = Y = a_{i,j}\chi_{i,j}$ where $a_{i,j} = \gamma_R P_j^{\text{tx}} d_{i,j}^{-\alpha}$. By using a single variable transformation, the PDF and CDF of Y can be given, respectively, as follows:

$$f_Y(y) = \frac{\lambda}{a_{i,j}} e^{-\frac{\lambda}{a_{i,j}} y}, \quad F_Y(y) = 1 - e^{-\frac{\lambda}{a_{i,j}} y}. \tag{4.8}$$

The interference $I_i = \sum_{k\neq j} P_k^{\text{tx}} \gamma_R d_{i,k}^{-\alpha} \chi_{i,k} = \sum_{k\neq j} b_{i,k}\chi_{i,k}$ follows Hypoexponential distribution [54] as I_i is the weighted sum of n independent but non-identical exponential random variables. Each exponential is scaled with a different factor due to the different distance between the CAV and the interfering BSs. The PDF of the interference can thus be given by:

$$f_{I_i}(I) = \sum_{k=1,k\neq j}^{N} \frac{\lambda}{b_{i,k}} e^{-\frac{\lambda}{b_{i,k}} I} \prod_{l=1,l\neq k} \frac{b_{i,k}}{b_{i,k} - b_{i,l}}, \tag{4.9}$$

Now, we define $X = N_R + I_i$. The PDF of X can be given after a single random variable transformation as $f_X(x) = f_I(x - N_R)$. Finally, given the statistics of X and

Y, we derive the PDF of $Z = Y/X$ [55] as:

$$\begin{aligned} f_Z(z) &= \int_0^\infty x f_X(x) f_Y(xz) dx \\ &= \sum_{k=1,k\neq j}^{N} \frac{\lambda^2 e^{\frac{\lambda N_R}{b_{i,k}}}}{a_{i,j}\, b_{i,k}} \prod_{l=1,l\neq k} \frac{b_{i,k}}{b_{i,k} - b_{i,l}} \int_0^\infty x e^{-\frac{\lambda}{a_{i,j}} xz - \frac{\lambda}{b_{i,k}} x} dx. \\ &= \sum_{k=1,k\neq j}^{N} \frac{a_{i,j}\, b_{i,k} e^{\frac{\lambda N_R}{b_{i,k}}}}{(b_{i,k} z + a_{i,j})^2} \prod_{l=1,l\neq k} \frac{b_{i,k}}{b_{i,k} - b_{i,l}}. \end{aligned} \tag{4.10}$$

Furthermore, the CDF of Z is as follows:

$$F_Z(z) = 1 - \sum_{k=1,k\neq j}^{N} \frac{a_{i,j} e^{\frac{\lambda N_R}{b_{i,k}}}}{b_{i,k} z + a_{i,j}} \prod_{l=1,l\neq k} \frac{b_{i,k}}{b_{i,k} - b_{i,l}}. \tag{4.11}$$

Finally, the outage in **Lemma 3** can be calculated by substituting $z = \gamma_{\text{th}}$ in (4.11).

□

In the following, we characterize the average HO-aware data rate using the statistics of SINR.

Lemma 4 (Ergodic HO-Aware Data Rate)**.** *Given the PDF and CDF of SINR, the closed-form ergodic rate expression can be given as follows:*

$$M_{\text{avg}}(\mu) = W(1 - \bar{h}_d \mu v) \sum_{k=1,k\neq j}^{N} \frac{\beta_k a_{i,j} e^{\frac{\lambda N_R}{b_{i,k}}}}{a_{i,j} - b_{i,k}} \prod_{l=1,l\neq k} \frac{b_{i,k}}{b_{i,k} - b_{i,l}}, \tag{4.12}$$

where $\beta_k = \ln(a_{i,j}/b_{i,k}) + \text{atan2}(\lambda/b_{i,k}, 0)$*, and* $\text{atan2}(y, x)$ *is the 2-argument arctangent function.*

Proof. We begin by defining the ergodic rate as follows:

$$\begin{aligned} M_{\text{avg}}(\mu) &= \mathbb{E}\left[W \log_2\left(1+Z\right)\left(1-\bar{h}_d \mu v\right)\right] \\ &= W(1-\bar{h}_d \mu v)\mathbb{E}\left[\log_2\left(1+Z\right)\right], \end{aligned} \tag{4.13}$$

where $\bar{h}_d = h_d/(\mu_{\max} V_{\max})$ and Z is a function of μ. Given the definition of ergodic rate [27], we have:

$$\begin{aligned} R_{\text{avg}}(\mu) &= \mathbb{E}\left[\log_2\left(1+Z\right)\right] = \int_0^{\infty} \log_2(1+Z) f_Z(z) dz, \\ &= \frac{1}{\ln(2)} \int_0^{\infty} \frac{1-F_Z(z)}{1+z} dz, \\ &= \frac{1}{\ln(2)} \int_0^{\infty} \sum_{k=1,k\neq j}^{N} \frac{a_{i,j} e^{\frac{\lambda N_R}{b_{i,k}}} \prod_{l=1,l\neq k} \frac{b_{i,k}}{b_{i,k}-b_{i,l}}}{(b_{i,k}+a_{i,j})z + b_{i,k} z^2 + a_{i,j}} dz, \end{aligned} \tag{4.14}$$

where (4.14) is a function of μ because $d_{i,j}, d_{i,k}$ and in turn $b_{i,j}, b_{i,k}$ are functions of μ. The final step is derived by substituting (4.11) into (4.14). The closed-form ergodic capacity can be derived by solving the integral as follows:

$$R_{\text{avg}}(\mu) = \sum_{k=1,k\neq j}^{N} \beta_k \frac{a_{i,j} e^{\frac{\lambda N_R}{b_{i,k}}}}{a_{i,j}-b_{i,k}} \prod_{l=1,l\neq k} \frac{b_{i,k}}{b_{i,k}-b_{i,l}}, \tag{4.15}$$

Finally, the HO-aware data rate can be given by substituting (4.15) into (4.13). □

To simplify the optimization, we also provide a worst-case bound on the interference.

Lemma 5 (Worst-Case Data Rate at CAV i)**.** *The worst-case signal power will be observed at a CAV when the CAV is located at the halfway point between two BSs (i.e.*

$\frac{1}{2\mu}$) *such that* $d_{i,j} = d_{\max} = \sqrt{h_{\text{bs}}^2 + d_{\text{safe}}^2 + \frac{1}{4\mu^2}}$. *The worst-case interference will also be observed at this location because the CAV will have maximum signal and interference from the neighbouring BSs such that.* $d_{i,k} = \sqrt{h_{\text{bs}}^2 + d_{\text{safe}}^2 + \frac{(2k+1)^2}{4\mu^2}}$. *Finally, the ergodic worst-case data rate is given as*

$$R_{\text{worst}}(\mu) = \sum_{k=1,k\neq j}^{N} \frac{\beta_k d_{\max}^{-\alpha} e^{\frac{\lambda N_R}{\gamma_R P_j^{\text{tx}} d_{i,k}^{-\alpha}}}}{d_{\max}^{-\alpha} - d_{i,k}^{-\alpha}} \prod_{l=1,l\neq k} \frac{d_{i,k}^{-\alpha}}{d_{i,k}^{-\alpha} - d_{i,l}^{-\alpha}}.$$

4.4 QoS- Constrained Traffic Flow Maximization

In this section, we formulate the macroscopic traffic flow maximization problem with various constraints to jointly optimize the CAV speed v and the active BS density μ in the presence of interference. Note that active BS density optimization can also be implemented in practice by dynamically switching the BSs. We present a closed-form expression for the optimal CAV speed and a numerical method to compute optimal μ.

The traffic flow maximization problem is formulated as:

$$\begin{aligned}
(\mathbf{P1}) \quad & \max_{v,\mu} \qquad Q = v \exp\left(\frac{\sigma_{\text{LN}}^2 - 2\mu_{\text{LN}}}{2}\right) \\
\text{s.t.}(\mathbf{C1}) \quad & v \leq \frac{\exp\left(\sigma_{\text{LN}}\sqrt{2}\,\text{erf}^{-1}\left(2\epsilon - 1\right) + \mu_{\text{LN}}\right)}{\tau} = V_{\text{safe}} \\
(\mathbf{C2}) \quad & v \leq \frac{1}{\bar{h}_d \mu}\left(1 - \frac{R_{\text{th}}}{W R_{\text{worst}}(\mu)}\right) = V_{\text{data}}(\mu) \\
(\mathbf{C3}) \quad & R_{\text{th}} \leq W R_{\text{worst}}(\mu) \\
(\mathbf{C4}) \quad & 0 < v \leq V_{\max} \\
(\mathbf{C5}) \quad & 0 \leq \mu \leq \mu_{\max}
\end{aligned}$$

where **C1** is the collision avoidance constraint which ensures that the speed of the CAVs should not exceed s/τ, i.e.,

$$\Pr\left(v \geq \frac{s}{\tau}\right) = \Pr\left(s \leq v\tau\right) \leq \epsilon, \tag{4.16}$$

where s is the distance between two CAVs and is always greater than zero, τ represents the processing time for the CAVs to act on a decision, and ϵ is the crash tolerance level. In addition, equation (4.16) can be rewritten by substituting the CDF of s where $\Pr\left(v \geq \frac{s}{\tau}\right) = \frac{1}{2}\left(1 + \text{erf}\left(\frac{\ln(v\tau) - \mu_{\text{LN}}}{\sigma_{\text{LN}}\sqrt{2}}\right)\right)$. By using the inverse error function and taking the inverse log of both sides and factoring for v, (4.16) can be rewritten as in **C1. C1** indicates that speed is capped to create an adequate safety distance that is traversed during the processing time. We refer to the right side of **C1** as the maximum safe speed that keeps the crash probability below ϵ. The condition **C1** shows that the maximum safe speed increases with ϵ, but decreases with the processing time.

Furthermore, **C2** is the worst-case HO-aware data rate constraint of the CAV based on **Lemma 5**, i.e.,

$$M_{\text{worst}} = W(1 - \bar{h}_d \mu v) R_{\text{worst}}(\mu) \geq R_{\text{th}}. \tag{4.17}$$

By factoring out for v we can rewrite (4.17) as in **C2**, where we refer to the right side of **C2** as the maximum speed, denoted by $V_{\text{data}}(\mu)$ that ensures the minimum data rate requirement of the CAVs. To ensure that **C2** does not attain negative values of speed and the problem remains feasible, we introduce the constraint **C3**. That is, **C3** ensures $\frac{R_{\text{th}}}{W R_{\text{worst}}(\mu)} \leq 1$. The final two constraints **C4** and **C5** cap the speed and active BS density to a maximum, respectively.

Note that problem **P1** is a non-linear programming problem due to constraints **C2** and **C3** which are a non-linear function of μ. To solve this problem, we first compute the optimal speed v^* which is then further maximized to optimize active BS density as in the following Lemma.

Lemma 6. *Given that Q is linearly increasing with v, and that v is bounded from $V_{\max}$, V_{safe}, and V_{data}, the optimal speed $v^*(\mu)$ is derived as the largest feasible speed that does not violate the three constraints, such that*

$$v^*(\mu) = \min\{V_{\max}, V_{\text{safe}}, V_{\text{data}}(\mu)\}, \tag{4.18}$$

The optimal active BS density μ^* can then be computed using the `fminbnd` *function in MATLAB which is based on golden-section search algorithm (GSS) [56]. The GSS method can find the global maximum or minimum of a unimodal function; whereas, it converges to a local maximum or minimum for a function containing multiple extrema [57]. GSS is a one-dimensional search that works by reducing the interval in a golden ratio range, where the minimum of the interval lies within the interval. In our case, we want to determine the optimal value of μ which maximizes V_{data}, so we provide fmindbnd function with the negative of V_{data} as the objective function. The algorithm has a computational complexity of $\mathcal{O}(\log n)$ [58]. If $\mu^* > \mu_{\max}$, we have $\mu^* = \mu_{\max}$. Also, if μ^* violates $R_{\text{th}} \leq WR_{\text{worst}}(\mu^*)$, the problem becomes infeasible.*

4.5 Numerical Results and Discussions

In this section, we validate the accuracy of the derived expressions through computer simulations. Furthermore, we demonstrate the sensitivity of optimal traffic flow by

changing key parameters such as crash tolerance level, data rate thresholds, interference, etc. Insights are extracted related to the optimal CAV speed and active BS density.

Unless stated otherwise, the values of the system parameters [24] are used in the following figures are listed herein. $V_{\max} = 30$ m/s, $\mu_{\max} = 0.01$ BSs/m, $h_d = 3$ s/HO, $R_{\text{th}} = 60$ Mbps, $W = 40$ MHz, $G_R^{\text{tx}} = 1$ dB, $G_R^{\text{rx}} = 1$ dB, $c = 3 \times 10^8$ m/s, $f_R = 2.1$ GHz, $N_R = 1.507 \times 10^{-13}$ W/m^2, $P_j^{\text{tx}} = 1$ W, $\alpha = 3$, $\lambda = 1$, $\epsilon = 1\%$, $\tau = 6 \times 10^{-3}$ sec, $\mu_{\text{LN}} = 0$, $\sigma_{\text{LN}} = 1$, $d_{\text{safe}} = 5$ m, $h_{\text{bs}} = 8$ m, $L_R = 2000$ m.

Fig. 4.2 and Fig. 4.3 demonstrate the outage probability (4.7) and ergodic capacity (4.15) as a function of μ for various CAV speeds. The analytical expression match perfectly with the simulation results. When μ increases, the outage increases and rate decreases due to increasing interference and HOs. Furthermore, higher speeds result in higher probability of outage and lower ergodic capacity when compared to lower speeds, which is due to more frequent HOs.

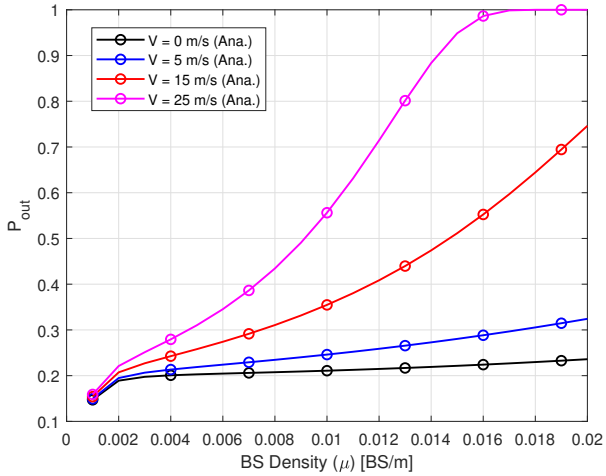

Figure 4.2: HO-aware rate outage probability as a function of μ for various speeds and $R_{\text{th}} = 1 \times 10^8$ bps, $\mu_{\max} = 0.02$ BSs/m.

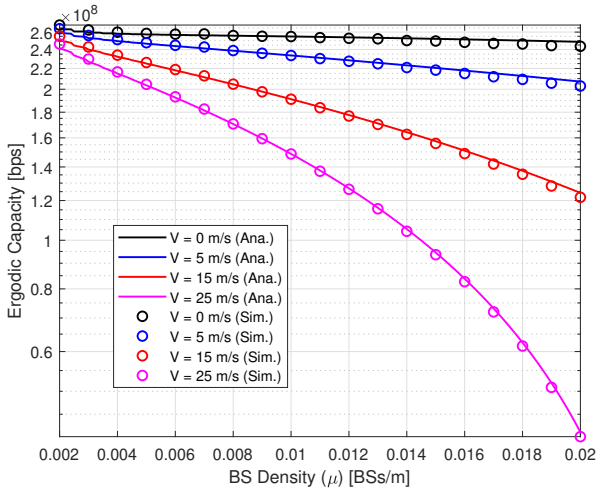

Figure 4.3: HO-aware capacity as a function of μ for various speeds for $R_{\text{th}} = 1 \times 10^8$ bps, $\mu_{\max} = 0.02$ BS/m.

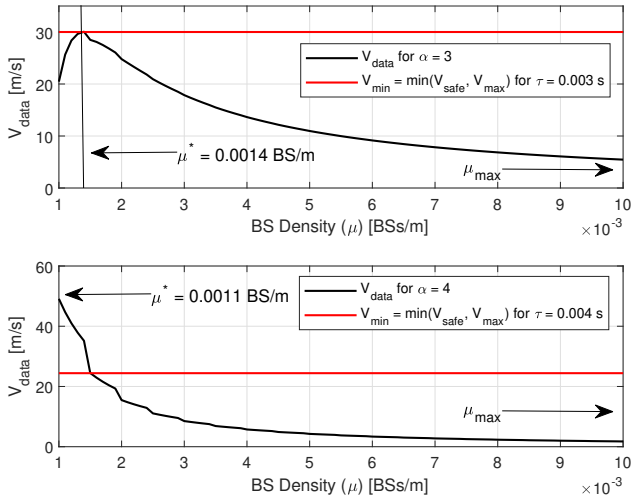

Figure 4.4: V_{data} as a function of μ for $\alpha = 3$ (Top) and $\alpha = 4$ (Bottom) with various CAV processing times τ.

Fig. 4.4 depicts V_{data} as a function of μ. As μ increases, V_{data} with $\alpha = 3$ increases up to a certain point due to vicinity of BSs. However, beyond that point V_{data} begins to decrease due to an increase in HOs and interference, and the CAVs need to lower their speed. On the other hand, when $\alpha = 4$, the benefit of rate enhancement cannot

be seen and a higher μ only causes more interference and HOs. Furthermore, we show that different CAV processing times τ varies V_{safe}, where $v^* = V_{\text{safe}}$ for higher τ values when $V_{\text{safe}} < V_{\text{data}}$.

Fig. 4.5 depicts the impact of the data rate threshold R_{th} on traffic flow Q and the optimal active BS density μ^* for various path-loss exponents. As seen on the top of Fig. 3.3, as R_{th} increases, Q decreases as CAVs need to reduce their speed to limit the number of HOs to meet the required data rate. For the same reason, when R_{th}, μ^* increases. The environments with higher path-loss exponents require more dense BS deployment. Note that we consider 100 points (or R_{th} values) along the x-axis between 6×10^7 bps and 8×10^7 bps to compute analytical traffic flow which requires to compute the optimal density of BSs μ^* numerically using MATLAB's fminbnd function at each R_{th} value. Therefore, minor fluctuations are observed due to numerical computations of μ^*.

Fig 4.6 depicts the relationship between the crash tolerance level ϵ and traffic flow Q for various CAV processing times. At first, $V_{\text{safe}} < V_{\text{data}} < V_{\max}$, thus the optimal speed is bound to V_{safe} as in Lemma 4, where V_{safe} increases as the crash intensity level ϵ increases since we are relaxing the crash tolerance. After a certain ϵ value, $V_{\text{safe}} > V_{\text{data}}$. The optimal speed is bound to V_{data} as in Lemma 4, which is constant with respect to ϵ and results in an upbound flat curve. For different CAV processing times τ, the point at which V_{data} takes over changes. When the CAV processing time is larger, V_{safe} is smaller since it takes a longer time for the CAV to process decisions compared to smaller τ values.

Finally, Fig 4.7 depicts the relationship between active BS density μ and traffic flow Q with various BS safety distances. At first, when the active BS density μ is

lower, $V_{\text{safe}} < V_{\text{data}} < V_{\max}$ so the optimal speed is bound to V_{safe} as in Lemma 4. V_{safe} is constant with respect to μ which results in an upbound flat curve. As μ increases, HOs and interference increases which lowers V_{data} to the point where $V_{\text{safe}} > V_{\text{data}}$ and the optimal speed is bound to V_{data} as in Lemma 4. For different BS safety distances d_{safe}, the switching point between V_{safe} and V_{data} changes because the further away the BS is from the CAV, V_{data} will decrease because of weak signal strength. Furthermore, the traffic flow without interference results in better traffic flow as compared to the traffic flow with interference as the interference deteriorates the data rate, CAV speed, and traffic flow.

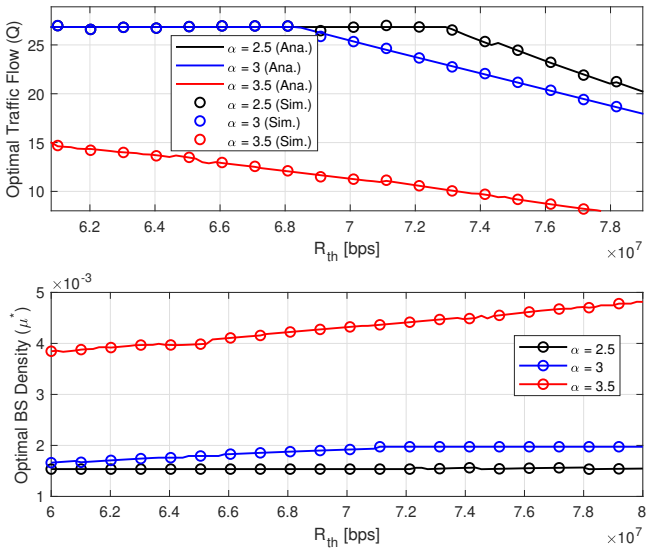

Figure 4.5: Traffic flow Q as a function of R_{th} with analytical and simulation results (Top) and optimal active BS density μ^* as a function of R_{th} (Bottom) for various path-loss exponents.

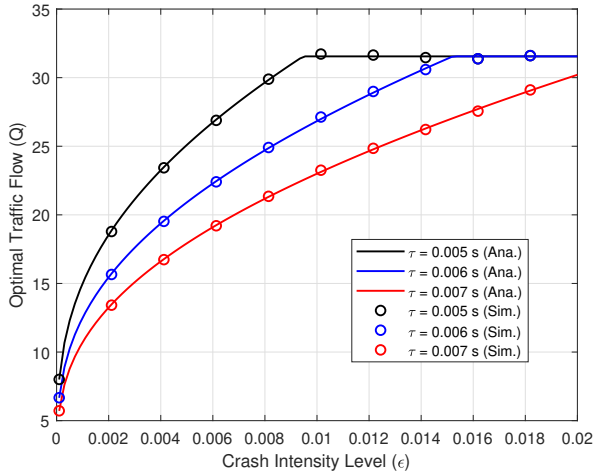

Figure 4.6: Traffic flow Q as a function of crash tolerance level ϵ and various CAV processing times τ.

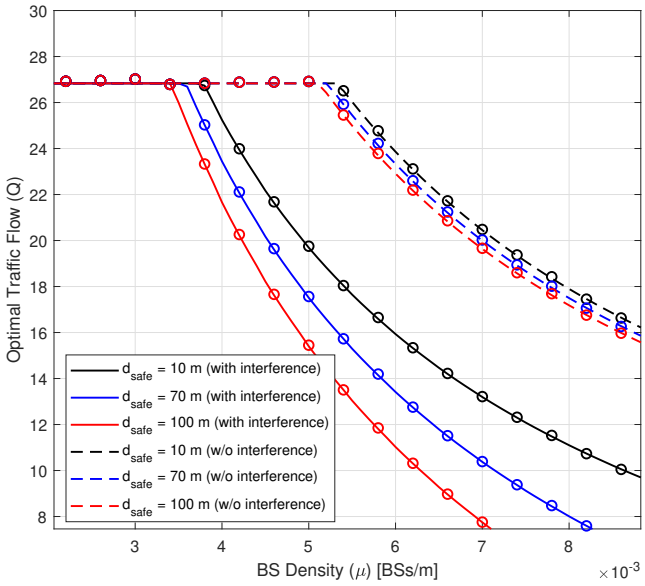

Figure 4.7: Traffic flow Q as a function of μ with various BS safety distances with and without interference.

4.6 Summary

This chapter presents a framework for V2I communications for CAVs where we present and analyze novel expressions for outage probability and ergodic capacity of HO-aware data rate, and jointly optimize the speed and network deployment in the presence of HOs between BSs and interference due to neighbouring BSs. Finally, we simulate and verify the results of the expressions through computer simulations, analyze the effect of mobility for outage probability and ergodic capacity of the HO-aware data rate, demonstrate the trade-off between achievable wireless data rates and traffic flow, and compare traffic flow with and without interference.

Chapter 5

Conclusions and Future Directions

5.1 Conclusion

This thesis provides a comprehensive framework for determining the optimal traffic flow by optimizing CAV speeds based on transportation and network constraints such as safety speed and HO-aware data rate. We propose a novel optimization problem for macroscopic traffic flow to jointly optimize the CAV speed and the density of BSs with and without considering interference. Furthermore, we propose an optimization problem to determine the optimal traffic flow using the microscopic car-following model based on Pipe's car-following model, where we optimize the speed of each individual CAV. Finally, we consider interference and the effect of the fading channel in the system model and derive novel closed-form expressions for outage probability and ergodic capacity of the HO-aware data rate. The numerical results validate all of the closed-form expressions, and provide useful insights such as the effect of active BS density on traffic flow, the comparison between macroscopic and microscopic traffic flow, the effect of mobility in outage probability, and finally the comparison between traffic flow with and without interference. We observed that dense BS deployment can

lead to an increase in handovers, which decreases the data rate, which decreases the traffic flow because the CAVs will travel at lower speeds. Furthermore, we noticed that the traffic flow in the presence of interference is generally lower compared to the traffic flow without interference, which provides a realistic depiction of dense BS deployment.

5.2 Future Directions

This thesis provides a comprehensive framework for traffic flow optimization considering a network model and car-following transportation model. We considered a single lane highway and equidistant BSs along the road in the system model which allowed us to obtain a simple, yet effective formulation for the handover rate which resulted in closed-form expressions for data rate, traffic flow, and optimal speed. This work can be extended to consider different road environments, rigorous handoff policies by deploying different types of BSs, and utilizing machine learning techniques for traffic flow prediction. The extensions are described as follows:

5.2.1 Road Environments

The future of CAVs will be fully autonomous in all road environments. Therefore, there is a large scope in considering different road environments for traffic flow optimization. In this thesis, the road is assumed to be a highway without any intersections or traffic lights, however considering rural areas would provide an interesting analysis for CAV traffic flow optimization.

5.2.2 Handoff Policies

There are different ways to consider handoffs of a user from one BS to another. This thesis only considers nearest BS association, however other associations such as power-based association can occur when there are different types of BSs on the road. For instance, in [24], the authors consider a hybrid RF and THz BS setup, and a handoff occurs based on a comparison of received signal strengths. Furthermore, this thesis assumes that the BSs are placed equidistant from each other which simplifies the handover rate expression, which may not always be the case in network deployment. Therefore, extending this work to consider randomly distributed BSs would provide a more rigorous framework for the HO-aware data rate.

5.2.3 Resource and Power Allocation

This thesis does not consider resource and power allocation optimization, however this thesis can be extended to include this. By considering resource allocation, the objective function would be non-convex, and would require more rigorous optimization techniques such as KKT, or deep learning techniques to solve the problem. The following series of works [59–61] utilizes deep learning for resource allocation, but does not consider mobility of users or traffic flow.

5.2.4 Machine Learning

This work can be extended to incorporate machine learning in different ways. For instance, in [33], Yan et al. use reinforcement learning to characterize network selection and CAV driving policies to minimize collisions. This reinforcement learning model can be extended to include safe driving policies and traffic flow rewards while

considering HO-aware data rates. Furthermore, deep learning traffic flow prediction models have been widely used in research [62–65]. By using temporal graph convolutional neural networks, the system model in this thesis can be utilized for handover rate prediction and traffic flow prediction while considering different types of BSs in the road network.

Bibliography

[1] O. Pattnaik and B. Pattanayak, "Security in vehicular ad hoc network based on intrusion detection system," *American Journal of Applied Sciences*, vol. 11, pp. 337–346, 2014.

[2] J. Levinson, J. Askeland, J. Becker, J. Dolson, D. Held, S. Kammel, J. Z. Kolter, D. Langer, O. Pink, V. Pratt, M. Sokolsky, G. Stanek, D. Stavens, A. Teichman, M. Werling, and S. Thrun, "Towards fully autonomous driving: Systems and algorithms," pp. 163–168, 2011.

[3] G. Martin, *Sustainability Prospects for Autonomous Vehicles: Environmental, Social, and Urban*, 2019.

[4] L. Hobert, A. Festag, I. Llatser, L. Altomare, F. Visintainer, and A. Kovacs, "Enhancements of V2X commun. in support of cooperative autonomous driving," *IEEE Commun. Magazine*, vol. 53, no. 12, pp. 64–70, 2015.

[5] C. Jung, D. Lee, S. Lee, and D. H. Shim, "V2X-commun.-aided autonomous driving: System design and experimental validation," *Sensors*, vol. 20, no. 10, 2020.

[6] S. Nikkel. Canadian cell towers map. [Online]. Available: https://www.ertyu.org/steven_nikkel/cancellsites.html?lat=54.369701&lng=-117.355957&zoom=5&type=Roadmap&layers=a&pid=0

[7] Y. Sheffi, *Urban transportation networks*. Prentice-Hall, Englewood Cliffs, NJ, 1985, vol. 6.

[8] A. Chaintreau, P. Hui, J. Crowcroft, C. Diot, R. Gass, and J. Scott, "Pocket switched networks: Real-world mobility and its consequences for opportunistic forwarding," 2005.

[9] "Crawdad Trace Dartmouth," [Online]. Available: https://crawdad.org/.

[10] T. Camp, J. Boleng, and V. Davies, "A survey of mobility models for ad hoc network research," *Wireless Commun. and Mobile Computing*, vol. 2, 2002.

[11] A. Einstein, *Investigations on the Theory of the Brownian Movement*, ser. Dover Books on Physics Series. Dover Publications, 1956. [Online]. Available: https://books.google.ca/books?id=AOIVupH_hboC

[12] I. Rhee, M. Shin, S. Hong, K. Lee, S. J. Kim, and S. Chong, "On the levy-walk nature of human mobility," *IEEE/ACM Trans. on Networking*, vol. 19, no. 3, pp. 630–643, 2011.

[13] F. Bai and A. Helmy, "A survey of mobility models," *Wireless Adhoc Networks. University of Southern California, USA*, vol. 206, p. 147, 2004.

[14] M. Sánchez and P. Manzoni, "Anejos: a java based simulator for ad hoc networks," *Future Generation Computer Systems*, vol. 17, no. 5, pp. 573–583,

2001. [Online]. Available: https://www.sciencedirect.com/science/article/pii/S0167739X00000406

[15] X. Hong, M. Gerla, G. Pei, and C.-C. Chiang, "A group mobility model for ad hoc wireless networks," in *Proceedings of the 2nd ACM International Workshop on Modeling, Analysis and Simulation of Wireless and Mobile Systems*, ser. MSWiM '99. New York, NY, USA: Association for Computing Machinery, 1999, p. 53–60. [Online]. Available: https://doi.org/10.1145/313237.313248

[16] L. A. Pipes, "Car following models and the fundamental diagram of road traffic," *Transportation Research*, vol. 1, pp. 21–29, 1967.

[17] M. Papageorgiou, "Some remarks on macroscopic traffic flow modelling," *Transportation Research Part A: Policy and Practice*, vol. 32, no. 5, pp. 323–329, 1998. [Online]. Available: https://www.sciencedirect.com/science/article/pii/S0965856497000487

[18] J. Popping, E. Begeleider, and T. Begeleider, "An overview of microscopic and macroscopic traffic models," 2013. [Online]. Available: https://fse.studenttheses.ub.rug.nl/11050/1/Bachelorproject.pdf

[19] F. Kessels, *Mesoscopic Models: Introduction to Traffic Flow Theory Through a Genealogy of Models*, 2019, pp. 99–106.

[20] B. D. Greenshields, J. T. Thompson, H. C. Dickinson, and R. S. Swinton, "The photographic method of studying traffic behavior," 1934.

[21] R. Arshad, H. Elsawy, S. Sorour, T. Y. Al-Naffouri, and M.-S. Alouini, "Handover management in 5G and beyond: A topology aware skipping approach," *IEEE Access*, vol. 4, pp. 9073–9081, 2016.

[22] D. Qu, X. Chen, W. Yang, and X. Bian, "Modeling of car-following required safe distance based on molecular dynamics," *Mathematical Problems in Engineering*, vol. 2014, pp. 1–7, 2014.

[23] X. Shi and X. Li, "Constructing a fundamental diagram for traffic flow with automated vehicles: Methodology and demonstration," *Transportation Research Part B: Methodological*, vol. 150, pp. 279–292, 2021.

[24] M. T. Hossan and H. Tabassum, "Mobility-aware performance in hybrid RF and Terahertz wireless networks," *IEEE Trans. on Commun.*, vol. 70, no. 2, pp. 1376–1390, 2022.

[25] C. E. Shannon, "A mathematical theory of commun." *The Bell System Technical Journal*, vol. 27, no. 3, pp. 379–423, 1948.

[26] H. Tabassum, M. Salehi, and E. Hossain, "Fundamentals of mobility-aware performance characterization of cellular networks: A tutorial," *IEEE Commun. Surveys & Tutorials*, vol. 21, no. 3, pp. 2288–2308, 2019.

[27] M. Monemi and H. Tabassum, "Performance of UAV-assisted D2D networks in the finite block-length regime," *IEEE Trans. on Commun.*, vol. 68, no. 11, pp. 7270–7285, 2020.

[28] G. Grimmett and D. Stirzaker, *Probability and random processes.* Oxford; New York: Oxford University Press, 2001. [Online]. Available: http://www.worldcat.org/search?qt=worldcat_org_all&q=9780198572220

[29] A. Ruszczynski, *Nonlinear Optimization.* Princeton University Press, 2011. [Online]. Available: https://doi.org/10.1515/9781400841059

[30] R. Arshad, H. ElSawy, S. Sorour, T. Y. Al-Naffouri, and M.-S. Alouini, "Velocity-aware handover management in two-tier cellular networks," *IEEE Trans. on Wireless Commun.*, vol. 16, no. 3, pp. 1851–1867, 2017.

[31] H. Ibrahim, H. ElSawy, U. T. Nguyen, and M.-S. Alouini, "Mobility-aware modeling and analysis of dense cellular networks with C-plane / U-plane split architecture," *IEEE Trans. on Commun.*, vol. 64, no. 11, pp. 4879–4894, 2016.

[32] X. Lin, R. K. Ganti, P. J. Fleming, and J. G. Andrews, "Towards understanding the fundamentals of mobility in cellular networks," *IEEE Trans. on Wireless Commun.*, vol. 12, no. 4, pp. 1686–1698, 2013.

[33] Z. Yan and H. Tabassum, "Reinforcement learning for joint V2I network selection and autonomous driving policies," in *IEEE Global Commun. Conference*, 2022, pp. 1241–1246.

[34] S. Jiao, S. Zhang, B. Zhou, Z. Zhang, and L. Xue, "Extended car-following model considering the drivers' characteristics under a V2V commun. environment," *Traffic Flow Modelling and Simulation towards Sustainable Transportation*, vol. 4, 2020.

[35] M. Nourinejad, S. Bahrami, and Y. Yin, "Optimal investment in driving automation: Individual vs. cooperative sensing," 2022. [Online]. Available: https://ssrn.com/abstract=4087061

[36] S. Nikhat and M. Mehmet-Ali, "A performance evaluation of millimeter-wave cellular networks with user mobility," in *2018 IEEE Canadian Conference on Electrical & Computer Engineering (CCECE)*, 2018, pp. 1–6.

[37] S. Choi, J.-G. Choi, and S. Bahk, "Mobility-aware analysis of millimeter wave commun. systems with blockages," *IEEE Trans. on Vehicular Technology*, vol. 69, no. 6, pp. 5901–5912, 2020.

[38] C. Chen and X. Zhao, "Mobility-aware access strategy in multi-user hetnets," *IEEE Wireless Commun. Letters*, vol. 9, no. 7, pp. 1004–1008, 2020.

[39] F. Guidolin, I. Pappalardo, A. Zanella, and M. Zorzi, "Context-aware handover policies in hetnets," *IEEE Trans. on Wireless Commun.*, vol. 15, no. 3, pp. 1895–1906, 2016.

[40] D. López-Pérez, Güvenç, and X. Chu, "Mobility enhancements for heterogeneous networks through interference coordination," in *2012 IEEE Wireless Commun. and Networking Conference Workshops (WCNCW)*, 2012, pp. 69–74.

[41] W. Bao and B. Liang, "Stochastic geometric analysis of user mobility in heterogeneous wireless networks," *IEEE Journal on Selected Areas in Commun.*, vol. 33, no. 10, pp. 2212–2225, 2015.

[42] S.-Y. Hsueh and K.-H. Liu, "An equivalent analysis for handoff probability in heterogeneous cellular networks," *IEEE Commun. Letters*, vol. 21, no. 6, pp. 1405–1408, 2017.

[43] T.-S. Dao, C. M. Clark, and J. P. Huissoon, "Distributed platoon assignment and lane selection for traffic flow optimization," in *2008 IEEE Intelligent Vehicles Symposium*, 2008, pp. 739–744.

[44] A. Talebpour and H. Mahmassani, "Influence of connected and autonomous vehicles on traffic flow stability and throughput," *Transportation Research Part C Emerging Technologies*, vol. 71, pp. 143–163, 2016.

[45] B. Si, J. Long, and Z. Gao, "Optimization model and algorithm for mixed traffic of urban road network with flow interference," *Science in China Series E: Technological Sciences*, vol. 51, no. 12, pp. 2223–2232, 2008.

[46] C. Wang, S. Gong, A. Zhou, T. Li, and S. Peeta, "Cooperative adaptive cruise control for connected autonomous vehicles by factoring commun.-related constraints," *Transportation Research Part C: Emerging Technologies*, vol. 113, pp. 124–145, 2020. [Online]. Available: https://www.sciencedirect.com/science/article/pii/S0968090X18317133

[47] Y. Qin, H. Wang, and B. Ran, "Impact of connected and automated vehicles on passenger comfort of traffic flow with vehicle-to-vehicle commun." *KSCE journal of civil engineering*, vol. 23, no. 2, pp. 821–832, 2019.

[48] S. Salman and S. Alaswad, "Alleviating road network congestion: Traffic pattern optimization using markov chain traffic assignment," *Computers & Operations Research*, vol. 99, pp. 191–205, 2018.

[49] J. G. Xian and D. Han, "The probability distribution of inter-car spacings," pp. 541–549, 2009.

[50] I. S. Gradshteyn and I. M. Ryzhik, *Table of integrals, series, and products*. Academic press, 2014.

[51] J. Sayehvand and H. Tabassum, "Interference and coverage analysis in coexisting RF and dense TeraHertz wireless networks," *IEEE Wireless Commun. Letters*, vol. 9, no. 10, pp. 1738–1742, 2020.

[52] R. Mahnke, J. Kaupužs, and I. Lubashevsky, "Probabilistic description of traffic flow," *Physics Reports*, vol. 408, no. 1, pp. 1–130, 2005.

[53] N. Wisitpongphan, F. Bai, P. Mudalige, V. Sadekar, and O. Tonguz, "Routing in sparse vehicular ad hoc wireless networks," *IEEE Journal on Selected Areas in Commun.*, vol. 25, no. 8, pp. 1538–1556, 2007.

[54] S. Khaled, T. Kadri, and S. Kadry, "Hypoexponential distribution with different parameters," *Journal of Applied Mathematics*, vol. 4, pp. 624–631, 04 2013.

[55] N. Jawad, A. Nasar, and J. Hadad, "Distributions of the ratio and product of two independent weibull and lindley random variables," *Journal of Probability and Statistics*, vol. 2020, 05 2020.

[56] W. H. Press, S. A. Teukolsky, W. T. Vetterling, and B. P. Flannery, *Numerical Recipes 3rd Edition: The Art of Scientific Computing*, 3rd ed. USA: Cambridge University Press, 2007.

[57] "Chapter 11 - basic methods," in *Numerical Methods and Optimization in Finance (Second Edition)*, second edition ed., M. Gilli, D. Maringer, and E. Schumann, Eds. Academic Press, 2019, pp. 229–271.

[58] D. E. Ferguson, "Fibonaccian searching," *Commun. ACM*, vol. 3, no. 12, p. 648, 1960.

[59] H. Zarini, A. Khalili, H. Tabassum, M. Rasti, and W. Saad, "Alexnet classifier and support vector regressor for scheduling and power control in multimedia heterogeneous networks," *IEEE Trans. on Mobile Computing*, 2021.

[60] S. Zarandi, A. Khalili, M. Rasti, and H. Tabassum, "Multi-objective energy efficient resource allocation and user association for in-band full duplex small-cells," *IEEE Trans. on Green Commun. and Networking*, vol. 4, no. 4, pp. 1048–1060, 2020.

[61] S. Zarandi and H. Tabassum, "Federated double deep Q-learning for joint delay and energy minimization in IoT networks," in *2021 IEEE International Conference on Commun. Workshops (ICC Workshops)*. IEEE, 2021, pp. 1–6.

[62] L. Yu, B. Du, X. Hu, L. Sun, L. Han, and W. Lv, "Deep spatio-temporal graph convolutional network for traffic accident prediction," *Neurocomputing*, vol. 423, pp. 135–147, 2021. [Online]. Available: https://www.sciencedirect.com/science/article/pii/S092523122031451X

[63] A. Essien, I. Petrounias, P. Sampaio, and S. Sampaio, "A deep-learning model for urban traffic flow prediction with traffic events mined from twitter," *World Wide Web*, vol. 24, 07 2021.

[64] M. Li, Y. Wang, Z. Wang, and H. Zheng, "A deep learning method based on an attention mechanism for wireless network traffic prediction," *Ad Hoc Networks*, vol. 107, p. 102258, 2020. [Online]. Available: https://www.sciencedirect.com/science/article/pii/S1570870519310923

[65] T. Mallick, P. Balaprakash, E. Rask, and J. Macfarlane, "Transfer learning with graph neural networks for short-term highway traffic forecasting," in *2020 25th International Conference on Pattern Recognition (ICPR)*, 2021, pp. 10 367–10 374.